Bayesian calibration for the Arctic sea ice biomarker IP_{25}

C.Y. Fu[1], M.B. Osman[1], and M.A. Aquino-López[1]

[1]Department of Geography, University of Cambridge, Cambridge, UK

Key Points:

- A new ln(PIP_{25}) index is proposed for fully quantitative sea ice reconstruction based on IP_{25} and associated phytoplankton biomarkers.
- Using a pan-Arctic core-top biomarker database, a Bayesian model is developed to calibrate the proxy nonlinearly to sea ice concentration.
- The calibration considers the non-stationary proxy seasonality and the influence of salinity for more accurate palaeoclimate inference.

Corresponding author: C.Y. Fu, cyf25@cam.ac.uk

Abstract

Sea ice plays multiple important roles in regulating the global climate. Rapid sea ice loss in the Arctic has been documented over recent decades, yet our understanding of long-term sea ice variability and its feedbacks remains limited by a lack of quantitative sea ice reconstructions. The sea ice diatom-derived biomarker IP_{25} has been combined with sterols produced by open-water phytoplankton in the PIP_{25} index as a sea ice proxy to achieve semi-quantitative reconstructions. Here, we analyse a compilation of over 600 published core-top measurements of IP_{25} paired with brassicasterol and/or dinosterol across (sub-)Arctic oceans to calculate a new $\ln(PIP_{25})$ index that correlates nonlinearly with sea ice concentration. Leveraging sediment trap and sea ice observational studies, we develop a spatially varying Bayesian calibration (*BaySIC*) for $\ln(PIP_{25})$ to account for its non-stationary relationship with sea ice concentration and other environmental drivers (e.g. sea surface salinity). The model is fully invertible, allowing probabilistic forward modelling of the $\ln(PIP_{25})$ index as well as inverse modelling of past sea ice concentration with bi-directional uncertainty quantification. *BaySIC* facilitates direct proxy-model comparisons and palaeoclimate data assimilation, providing the polar proxy constraints currently missing in climate model simulations and enabling, for the first time, fully quantitative Arctic sea ice reconstructions.

Plain Language Summary

A lipid termed IP_{25} is produced by microorganisms residing in Arctic sea ice and deposited in underlying sediments. By measuring its concentration in sediment cores, palaeoclimatologists can interpret past sea ice conditions at the core locations. When multiple cores across the Arctic are analysed, palaeo sea ice extents can be reconstructed. This study refines the quantitative relationship of this proxy with sea ice, taking into account seasonal biases and other influencing environmental factors. A Bayesian (probabilistic) approach is used to quantify the uncertainties in the calibration. The new model enables quantitative Arctic sea ice reconstructions and helps us understand its long-term variability.

1 Introduction

Sea ice is a key component of the climate system, affecting planetary albedo (Curry et al., 1995), air-sea gas and heat exchanges (Ivanov et al., 2019; Rysgaard et al., 2011), and the thermohaline circulation (Mauritzen & Häkkinen, 1997), with impacts extending far beyond the polar regions. In recent decades, rising temperatures in the Arctic, caused by anthropogenic greenhouse gas emissions and amplified by the ice-albedo feedback, have led to rapid sea ice loss (Stroeve & Notz, 2018), yet our understanding of its long-term variability remains limited by our short-term observations (de Vernal et al., 2020). Furthermore, future projections for the Arctic Ocean suggest that it will become practically ice-free in summer at least once before the year 2050 under all emission scenarios, but the multi-model spread in simulated sea ice extent remains wide (Notz & SIMIP Community, 2020). To better understand changes in sea ice and associated feedbacks, as well as to improve predictions, quantitative palaeo sea ice reconstructions are needed.

Numerous proxies in marine sediment cores have been used to infer past sea ice conditions (e.g. de Vernal, Gersonde, et al., 2013), among which IP_{25} (Ice Proxy with 25 carbon atoms) is one of the most commonly employed. The highly branched isoprenoid (HBI) monoene is produced by sympagic diatoms during the spring sea ice algal bloom and released into the water column in early summer when sea ice melts (Belt et al., 2007, 2008, 2013; Brown et al., 2011, 2016). Having been detected in sediments across the Arctic, IP_{25} has been used as a proxy for seasonal sea ice in palaeo reconstructions extending as far back in time as the late Miocene (Stein et al., 2016). Within the Arctic and sub-Arctic regions, the absence of IP_{25} has been attributed to two opposing scenarios. On the one hand, it may reflect year-round ice-free conditions, which do not support the growth of IP_{25} producers (Belt et al., 2007; Belt & Müller, 2013; Müller et al., 2011). On the other hand, perennial sea ice cover has been hypothesised to hinder diatom growth by reduced light penetration through thick and dense ice (Belt et al., 2007; Belt & Müller, 2013; Müller

et al., 2009, 2011). This would limit the presence of IP_{25} close to the ice edge or in the marginal ice zone (MIZ; Müller et al., 2009, 2011).

To differentiate between the two contrasting sea ice conditions that preclude IP_{25} production, pelagic phytoplankton biomarkers have been used as indicators of (seasonal) open water conditions (e.g. Müller et al., 2009, 2011; Navarro-Rodriguez et al., 2013; Volkman, 1986; Volkman et al., 1998). These include brassicasterol (24-methylcholesta-5,22E-dien-3β-ol) and dinosterol (4α,23,24-trimethyl-5α-cholest-22E-en-3β-ol), which are mainly derived from diatoms, haptophytes, cryptophytes, and dinoflagellates during the summer phytoplankton bloom (e.g. Goad et al., 1983; Volkman, 1986; Volkman et al., 1993, 1998). Müller et al. (2011) first proposed coupling them with IP_{25} in the PIP_{25} (phytoplankton-IP_{25}) index to achieve quantitative sea ice reconstructions. The index is calculated as follows:

$$PIP_{25} = \frac{[IP_{25}]}{[IP_{25}] + c\ [\text{phytoplankton biomarker}]}, \tag{1}$$

where c is conventionally taken as the ratio of the mean IP_{25} and phytoplankton biomarker concentrations of the sediment samples under study. This factor was introduced to compensate for the substantial difference between the concentrations of IP_{25} and phytoplankton biomarkers: the former is typically lower, ascribed to its source-specificity in contrast to the multiple origins of the latter (Müller et al., 2011; Navarro-Rodriguez et al., 2013).

The PIP_{25} index is, by definition, limited between 0 and 1. As described by Belt and Müller (2013), high PIP_{25} values result from high IP_{25} and low sterol concentrations, indicative of predominantly ice-covered conditions; conversely, low PIP_{25} values arise from low IP_{25} and high sterol concentrations, which suggest mostly ice-free conditions. Intermediate PIP_{25} values are taken to represent ice-margin conditions. In addition to distinguishing between opposite sea surface conditions, the sterols serve a second role in the PIP_{25} index as proxies for productivity in the surface ocean (Müller et al., 2011; Belt & Müller, 2013). By normalising IP_{25} against primary productivity, PIP_{25} indices can be compared across different Arctic regions.

To realise the full potential of the PIP_{25} index in quantitative Arctic sea ice reconstructions, a robust calibration is needed. Since the initial ~~calibration~~correlation reported by Müller et al. (2011), numerous studies have been undertaken to improve and validate the model's applicability in different regions (e.g. Kolling et al., 2020; Navarro-Rodriguez et al., 2013; Stoynova et al., 2013; Xiao et al., 2013, 2015) and in deep time (e.g. Hoff et al., 2016; Knies et al., 2014; Kremer, Stein, Fahl, Bauch, et al., 2018; Kremer, Stein, Fahl, Ji, et al., 2018; Stein & Fahl, 2013; Stein et al., 2016, 2017), yet problems associated with the c factor and regional variability persist, hindering the wider use of this proxy. Furthermore, while possible influences of other environmental variables (e.g. salinity) on biomarker production and preservation have been acknowledged (Belt, 2018; Ribeiro et al., 2017; Xiao et al., 2013, 2015), they have rarely been included in calibrations, potentially underrating the aptness of PIP_{25} for reconstructing sea ice conditions (Su et al., 2022). As new biomarker datasets continue to be published and our understanding of the proxy system evolves, existing calibrations need to be revisited to take into account such evidence and insights, which may further help address previously identified issues.

At the same time, recent advances have been made in proxy system model (PSM) development using Bayesian statistical methods, with forward and inverse models developed for several commonly used marine geochemical palaeoclimate proxies (e.g. Malevich et al., 2019; Tierney & Tingley, 2014, 2018; Tierney et al., 2019). The probabilistic approach employed by these models enables more rigorous quantification of calibration uncertainties and their propagation into proxy estimates or climate reconstructions. In addition, such PSMs facilitate proxy-model comparisons (e.g. Hoem et al., 2022) and palaeoclimate data assimilation (e.g. Osman et al., 2021), allowing the use of proxy data to validate or constrain model simulations.

Here, we develop a Bayesian calibration for IP_{25} (and associated phytoplankton biomarkers) to model the relationship between the sea ice proxy and environmental factors using recently

compiled pan-Arctic biomarker, sea ice and oceanographic variable datasets~~, with~~. The Bayesian framework supports uncertainty quantification and propagation to model predictions in both the forward and inverse directions. The model, called *BaySIC* (Bayesian Sea Ice Concentration), is amenable to incorporating additional core-top data as they become available, as well as other environmental drivers that may be identified in future investigations. We demonstrate its applications with examples and discuss implications for palaeo-sea ice reconstruction.

2 Data Compilation

2.1 Biomarkers in Surface Sediments

We update the pan-Arctic surface biomarker database of Kolling et al. (2020) (Belt et al., 2013, 2015; Méheust et al., 2013; Müller et al., 2011; Navarro-Rodriguez et al., 2013; Pieńkowski et al., 2017; Smik et al., 2016; Xiao et al., 2013, 2015) with paired IP_{25}-brassicasterol and -dinosterol core-top measurements from recent literature (Harning et al., 2023), including the location (water depth, latitude, longitude), total organic carbon (TOC) content, and concentrations of the biomarkers normalised to gram of sediment (µg/gSed) and/or TOC (µg/gTOC). The expanded database consists of 644 surface sediment samples collected between 38.00°N and 89.98°N and across the full range of longitudes (figure 1; dataset S1). Samples within the same sea ice grid cell (see section 2.2) are averaged to avoid overrepresenting densely sampled areas. This results in 551 effective core-top samples with paired IP_{25}-brassicasterol measurements and 432 with paired IP_{25}-dinosterol measurements for our calibration model.

A dataset published by Stoynova et al. (2013) was excluded from the Kolling et al. (2020) database as it was obtained with different biomarker extraction solvents and method, and contained measurements inconsistent with those of other studies in the same area (e.g. Navarro-Rodriguez et al., 2013; Xiao et al., 2015). More recently, a dataset for the East Siberian Sea was made available by Su et al. (2022). However, it records distinct brassicasterol and dinosterol distributions, with the former more closely resembling the IP_{25} distribution. The authors hypothesised that the divergence emerged from differential impacts of estuarine turbidity on the respective sterol producers, but this is not observed in other datasets from river mouth settings (e.g. Xiao et al., 2013, 2015). In comparing the brassicasterol/dinosterol ratio of each dataset, we find that the Su et al. (2022) data deviates from the rest of the database (figure S1). Since the cause of this discrepancy remains conjectural, we refrain from incorporating this dataset into our database.

As biomarker concentrations are affected by sedimentation rates, it has been recommended that they be normalised to TOC contents prior to comparisons across space and time (Müller et al., 2011). The PIP_{25} index approach further circumvents comparing absolute concentrations by considering relative concentrations. When calculating PIP_{25}, the same normalisation should be applied to both the phytoplankton biomarker and IP_{25} concentrations. Since the normalisation factors are cancelled out in the ratios (Belt, 2018), PIP_{25} indices computed from measurements normalised in either way are directly comparable. However, as the biomarker concentrations are typically several magnitudes lower when normalised to gram of sediment rather than TOC content, the reported measurements are less precise, especially near the detection limit. We therefore use measurements reported in µg/gTOC where available for our calibration.

Both brassicasterol and dinosterol are commonly used as the phytoplankton biomarker in the PIP_{25} index (P_BIP_{25} and P_DIP_{25}, respectively) and, in general, their distributions are similar across the Arctic (figure 1). However, the sources of brassicasterol are more diverse than those of dinosterol: the former is produced by a range of marine and freshwater phytoplankton as well as higher plants (Volkman, 1986), while the latter is mainly synthesised by marine dinoflagellates (Nichols et al., 1984; Volkman et al., 1993, 1998). Brassicasterol found in marine sediments may have been transported by rivers from a lacustrine or terrestrial origin (Fahl et al., 2003; Hörner et al., 2016), thus appearing in higher concentrations than expected for the local sea surface conditions. Brassicasterol may also originate from sea ice diatoms (Belt et al., 2013, 2018), potentially undermining its role as an open ocean proxy. We develop calibrations for both P_BIP_{25} and

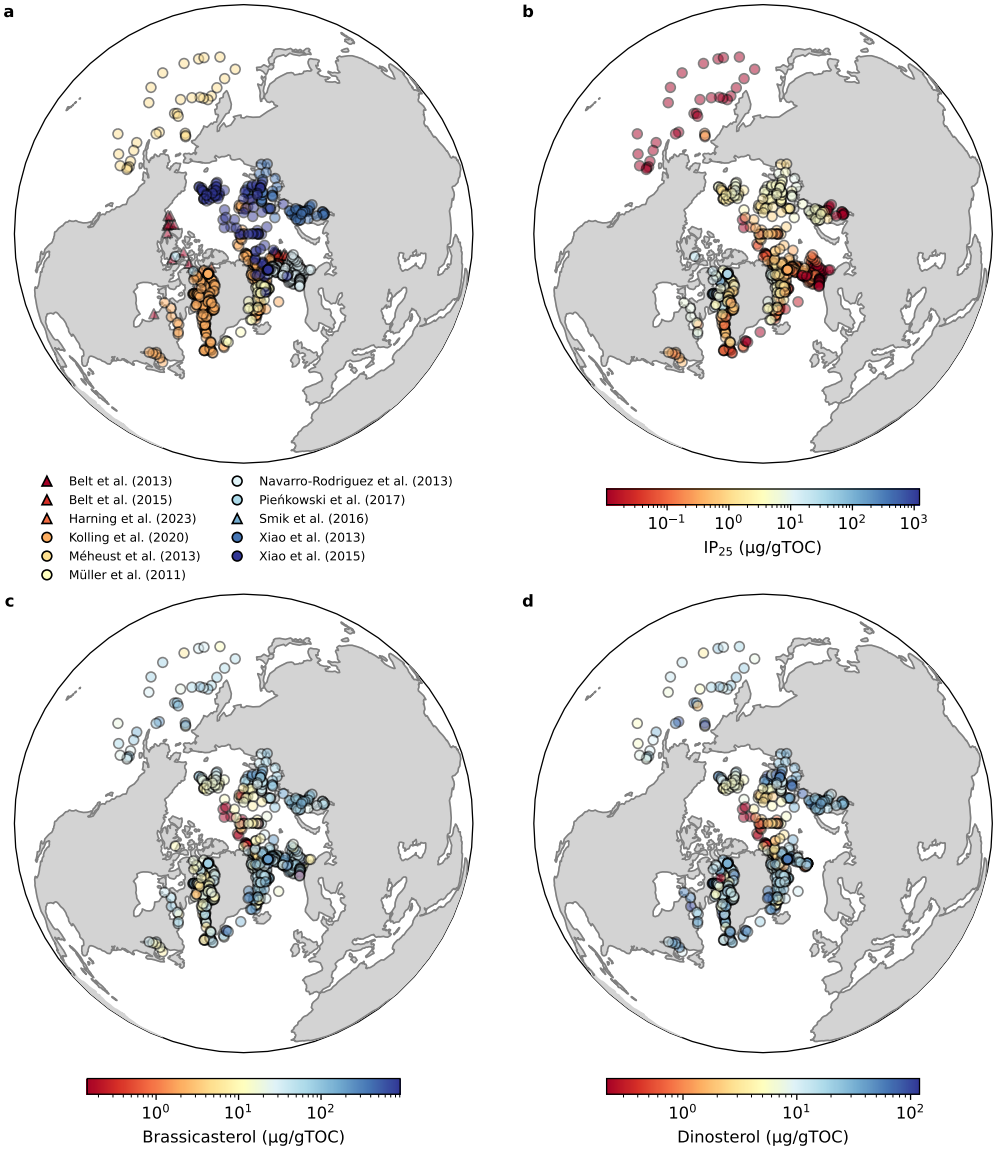

Figure 1. Locations of published core-top paired IP_{25} and brassicasterol and/or dinosterol measurements, coloured by (a) study of origin, and concentration of (b) IP_{25}, (c) brassicasterol, and (d) dinosterol, normalized to total organic carbon content (µg/gTOC). In (a), triangle = concentration normalised to gram of sediment only, and circle = concentration normalised to TOC content also available.

158 P_DIP_{25} but, due to the broader and more variable sources of brassicasterol, focus the discussion
159 on the latter.

160 We note that the sterol extraction method (with dichloromethane/methanol) used across all
161 studies has recently been suggested to underestimate concentrations (Köseoğlu, 2019) (figure S2).
162 However, since sterol data obtained with the more comprehensive method (using potassium hy-
163 droxide) remain limited, and as only relative concentrations are of importance for their role as
164 a normalisation factor in the PIP_{25} index, measurements acquired with the conventional method
165 are used here for the calibrations in order to investigate Arctic-wide trends and to maintain con-
166 sistency across datasets. Should sufficient data collected with the saponification step become avail-
167 able in the future, the calibrations may be updated to correct for any inaccuracies in the existing
168 core-top sterol concentrations.

169 ### 2.2 Sea Ice

170 Sea ice concentrations (SIC) corresponding to the core-top measurements are taken from
171 the NOAA/NSIDC Climate Data Record of Passive Microwave Sea Ice Concentration, Version
172 4 (Meier et al., 2021). The data are on a 25 km × 25 km grid and represent the percentage of ocean
173 surface area covered by sea ice. For each core location, the monthly SIC from January 1979 to
174 December 2022 in the nearest grid cell are drawn. The great-circle distance between each biomarker
175 measurement and SIC observation is less than 100 km in all but seven cases. Among these, six
176 samples are taken from locations in the North Pacific Ocean beyond the data coverage. The matched
177 SIC data indicate year-round ice-free conditions, as expected for these localities; thus, the sam-
178 ples are retained in our analysis. The remaining sample in Lake Melville is paired with SIC data
179 for the ocean and is consequently excluded from the database. Climatologies are created by com-
180 puting the mean monthly SIC from 1979 to 2000 and from 1979 to 2022. In each case, the in-
181 terquartile range (IQR) is also computed as a non-parametric measure of year-to-year sea ice vari-
182 ability.

183 Complementary SIC datasets are obtained from the Gridded Monthly Sea Ice Extent and
184 Concentration product, Version 2 (Walsh et al., 2019), which combines various historical sources
185 such as ship reports, maps by oceanographers, charts from meteorological institutes, etc. to pro-
186 vide an Arctic-wide SIC record from 1850 onwards. The data are on a 1/4° × 1/4° grid, and the
187 same procedures are followed to produce climatologies for the core locations. Since the prod-
188 uct builds on more complete sea ice observations from 1953, we generate climatologies from 1950
189 to 2000 and from 1950 to 2017.

190 ### 2.3 Sediment Trap Time Series

191 To explore proxy seasonality, we also collate measurements of IP_{25} fluxes in nine sediment
192 traps deployed across the Arctic (Bai et al., 2019; Belt et al., 2008; Gal et al., 2022; Koch et al.,
193 2020; Luostarinen et al., 2023; Nöthig et al., 2020; Rontani et al., 2016) (figure 2). Where mul-
194 tiple traps positioned at the same location are found, data from the deepest one are taken to more
195 closely reflect the fluxes that eventually reach the sediments. Each trap has a different sampling
196 period, ranging from one month to a year (see table S1 for details). We focus on the spring and
197 summer months, when IP_{25} is produced and released. Since the time series are approximately
198 normally distributed, we fit a normal probability density function (PDF) to each of them to fa-
199 cilitate composite analysis. Monthly SIC during the sampling period are extracted from the NOAA/NSIDC
200 record. In each case, data from grid cells within a 100 km radius of the trap location are com-
201 piled to assess regional sea ice variability and to account for lateral advection (Salter et al., 2023).
202 For sediment traps in the eastern Fram Strait, the source areas simulated by Salter et al. (2023)
203 spanned sea ice conditions from completely ice-free to mostly ice-covered at any given time
204 during the sampling period. To avoid dilution of the seasonal signal by lateral transport, we
205 exclude data from this area, including those previously collected by Lalande et al. (2016), from
206 our composite analysis.

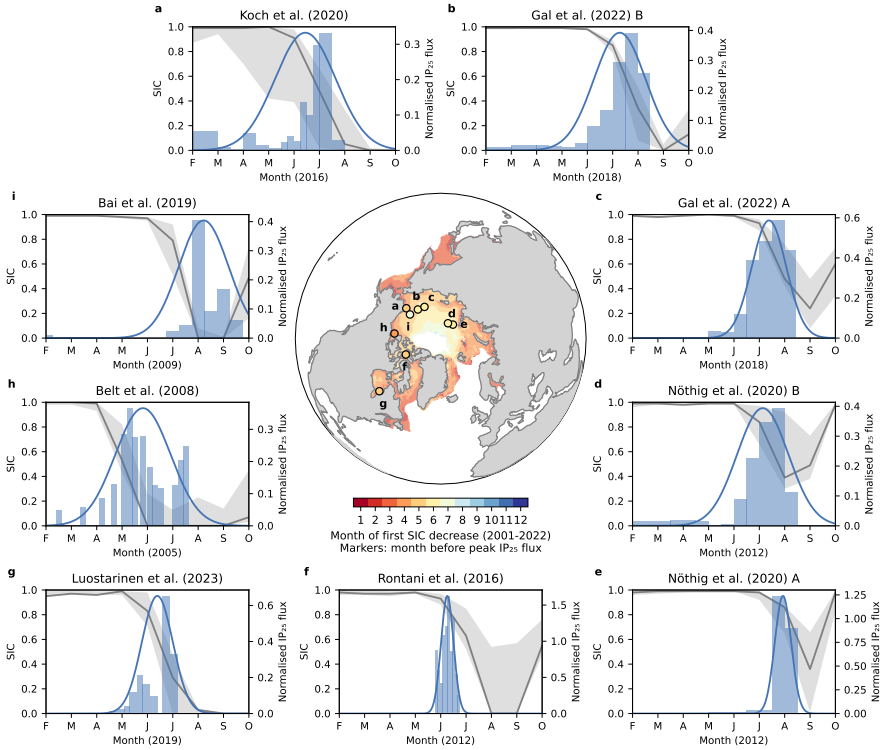

Figure 2. (a-i) Sediment-trap IP_{25} flux time series and the fitted normal probability density function, as well as the corresponding sea ice concentration (SIC) trend and uncertainty associated with lateral transport (range of SIC found within a 100 km radius). The map shows the location of each sediment trap coloured by the corresponding timing of the peak IP_{25} flux, and spatial variations in the timing of the first SIC decrease (2001-2022, matching the sampling periods of the sediment traps).

2.4 Oceanographic Variables

Environmental parameters such as temperature, salinity, and nutrient levels may promote or limit productivity, exerting additional influence on biomarker concentrations. To test for any such effects, measurements of these variables are acquired from World Ocean Atlas 2018 (Boyer et al., 2018; Garcia et al., 2019; Locarnini et al., 2019; Zweng et al., 2019). Temperature and salinity data are available at quarter-degree grid resolution, while silicate, nitrate, and phosphate data are available at one-degree grid resolution. Each core location is matched to the nearest grid cell to derive the monthly climatologies. For temperature and salinity, these are averages of six decadal means from 1955 to 2017; for the nutrients, these are averages of all available data. Data from the top 10 m of the water column (at 0 m, 5 m, and 10 m water depth) are averaged to represent sea surface conditions.

3 Data Exploration

3.1 Nonlinearity of the PIP_{25} Index

Following previous studies (e.g. Müller et al., 2011; Navarro-Rodriguez et al., 2013; Kolling et al., 2020), we investigate the relationship between PIP_{25} and SIC by assessing their correlation across space in contemporary records. Existing calibrations have sought to establish a positive linear relationship between the two by invoking the balance factor, c; however, complications arise with its use. For example, the factor has been found to vary both as a function of core section and location (e.g. Belt et al., 2015; Navarro-Rodriguez et al., 2013), such that the PIP_{25} value for a given sediment sample changes with the particular dataset under consideration. This necessitates the recalculation of PIP_{25} in each investigation that expands a previous dataset, which affects the inferred SIC. As Belt and Müller (2013) pointed out, the approach is particularly problematic for applications on geologic time scales, as the c factor may change significantly with the length of the core under study. Furthermore, the factor is susceptible to negative impacts of outlying biomarker measurements (Navarro-Rodriguez et al., 2013). Due to these unresolved issues, the PIP_{25} index has thus far remained a semi-quantitative proxy for sea ice.

Another difficulty in applying linear calibration models for past sea ice reconstruction lies in the highly variable slope and intercept across different regions (e.g. Müller et al., 2011; Smik et al., 2016; Xiao et al., 2015). To aid interregional comparisons, Xiao et al. (2015) proposed Arctic-wide c values (0.11 for P_DIP_{25}), which were subsequently updated by Kolling et al. (2020) using a larger dataset (0.203). Although similar values (0.238) can be calculated for our expanded database, marked regional differences persist in the linear correlation with SIC (not shown), preventing a pan-Arctic calibration. More generally, we show that the relationship between PIP_{25} and SIC remains nonlinear following correction across a broad range of c factors (figures 3a and S3). Thus, while the exact value taken for such a uniform factor may be revised by future core-top studies, it is unlikely that the relationship can ever be fully linearised.

In light of the problems associated with the c factor, we omit its use to develop a robust calibration. To reduce the positive skewness of the PIP_{25} data (calculated without c), we transform the ratio using the natural logarithmic function. The index then becomes:

$$\ln(\mathrm{PIP}_{25}) = \ln\left(\frac{[\mathrm{IP}_{25}]}{[\mathrm{IP}_{25}] + [\text{phytoplankton biomarker}]}\right), \tag{2}$$

where the phytoplankton biomarker is either brassicasterol or dinosterol. Our dataset contains samples where IP_{25} and/or the sterols are not detected. Although the biomarkers are recorded as absent in these cases, they may be present at concentrations below their respective limits of detection, which are expected to vary between laboratories but are rarely reported. Thus, the minimum non-zero IP_{25} concentration in the dataset, taken as the best approximation of the detection limit, is added to all IP_{25} measurements to enable the log transformation. The same treat-

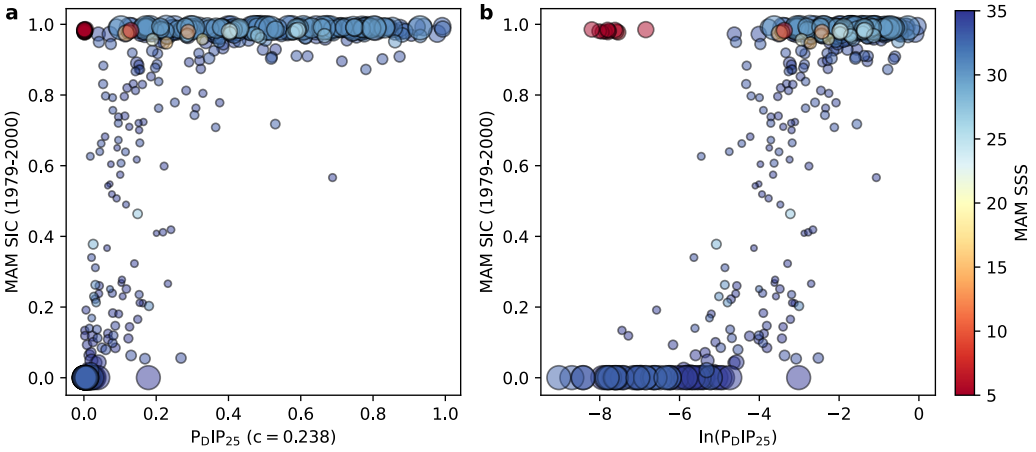

Figure 3. Mar-Apr-May sea ice concentration (SIC), 1979-2000, vs. (a) P_DIP_{25} calculated with the *c* factor and (b) ln(P_DIP_{25}), coloured by sea surface salinity (SSS). Bubble size is inversely proportional to the interquartile range of the SIC over the 22-year calibration period.

ment is applied to brassicasterol and dinosterol measurements to maintain consistency in the ratio.

Using our expanded database, which includes samples from permanently ice-free and ice-covered regions in the sub-Arctic and central Arctic, we find that the new ln(PIP_{25}) index exhibits a sigmoidal (i.e., logistic-like) relationship with SIC: as ln(PIP_{25}) approaches 0, SIC tends to 1; likewise, as ln(PIP_{25}) approaches negative infinity, SIC tends to 0 (figure 3b). The suitability of the logistic function in describing the relationship can be understood intuitively, as SIC values are inherently limited between 0 and 1. There is a clear transition from SIC = 0 to 1 at ln(PIP_{25}) ~ -4, which mirrors the relatively narrow MIZ in nature. As illustrated subsequently, this abrupt shift can be well-characterised by logistic regression coefficients, enabling more effective differentiation between ice-free and ice-covered conditions based on ln(PIP_{25}) values. Nevertheless, some variability is still evident in the the core-top data. This may be partly attributable to the inherent ambiguity of the PIP_{25} ratio: the same value can be derived from coevally high or low concentrations of IP_{25} and sterols, caused by different sea ice conditions (Müller et al., 2011). To mitigate this, it has been recommended that individual biomarker records be interpreted along with PIP_{25} (Belt & Müller, 2013; Müller et al., 2012).

3.2 Uncertainties in SIC Observations

As the proxy signals are taken to reflect the dominant sea ice conditions over the calibration period, ln(PIP_{25}) is compared against the climatological mean SIC. However, near the ice edge, the year-to-year variability in SIC can be significant: a location may be completely ice-covered in one year and ice-free in the next. In such cases, the core-top ln(PIP_{25}) value represents a mixture of variably recorded opposing sea ice conditions, and its relationship with the corresponding mean SIC value is uncertain. To incorporate this source of uncertainty in the calibration, we calculate the IQR of the SIC data over the calibration period as a non-parametric measure of its year-to-year variability (figure 3). Data points with high IQR values (high SIC variability) are associated with more uncertainties and thus are considered less reliable in the regression.

Although the core tops mostly sample the same sediment interval (1 cm, with exceptions in datasets from Harning et al. (2023) and Kolling et al. (2020)), as sedimentation rates across the Arctic and sub-Arctic oceans span a wide range, the samples would have accumulated over different periods, ranging from a few years to several millennia (Stein, 2008; Wegner et al., 2015).

As a result, most of the core tops represent coarse time composites that cannot be paired with SIC data over the same period. Considering the accelerated sea ice loss over the last couple of decades (Stroeve & Notz, 2018), we avoid using SIC data from this period in our calibration to prevent the potential overrepresentation of anthropogenic signals. The period 1979-2000 is hence chosen to maximise the limited satellite observations available. This means that samples recently collected from regions with high sedimentation rates (>0.1 cm/year) may be mismatched with SIC from an earlier period; however, such rapid sediment deposition is rare in the Arctic (Stein, 2008; Wegner et al., 2015). In our database, only Belt et al. (2015) reported accumulation rates of this order, for sites in the Barents Sea. In general, all matched SIC values remain estimates of the real conditions recorded by the core tops, with the largest discrepancies expected in areas that experienced dramatic SIC changes over recent decades to centuries (e.g. the MIZ). The full satellite SIC record (1979-2022) and datasets derived from historical sources (1950-2000 and 1950-2017) are also used to evaluate model sensitivity to the calibration period.

Pairing core-top biomarker measurements with SIC observations from the nearest satellite grid assumes minimal lateral transport. This assumption is valid in ice-covered regions, such as the Eurasian Basin, where vertical transport has been shown to account for the majority of the carbon fluxes to the sediments (Belt & Müller, 2013; Legendre et al., 1992; Nöthig et al., 2020). In other locations, however, lateral advection and resuspension have been found to affect biomarker fluxes, for example, on the Lomonosov Ridge (Fahl & Nöthig, 2007; Fahl & Stein, 2012) and in the eastern Fram Strait (Lalande et al., 2016; Salter et al., 2023). By modelling particle trajectories, Salter et al. (2023) showed that a source area could have a radius of approximately 100 km. This particularly complicates the interpretation of samples near the MIZ, where such a large integration area may span the full gradient of SIC values, resulting in a mixed proxy signal. In reality, due to variable lateral transport rates across the Arctic, each core top likely integrates biomarker fluxes over a different area, which may also have changed through time. As this source of uncertainty is poorly constrained, we do not explicitly include it in our model; nonetheless, it mainly affects core tops near the ice edge, which are already down-weighted in the regression based on their IQR values.

3.3 Spatiotemporal Variation in Proxy Seasonality

Given that biomarker production and IP_{25} release primarily occur during algal blooms and ice melt, respectively (Belt et al., 2008, 2013; Brown et al., 2011, 2016), the proxies are biased towards seasonal sea ice conditions (figure 4a-b). As sympagic algal blooms, sea ice thawing, and pelagic algal blooms do not occur simultaneously, the seasonal signal recorded by $\ln(PIP_{25})$ is a mixture of these timings and is not straightforward to characterise. Previous calibrations assumed a stationary proxy seasonality, usually towards spring (March-April-May or April-May-June, e.g. Müller et al., 2011; Navarro-Rodriguez et al., 2013; Smik et al., 2016). However, some studies also found good correlations between the PIP_{25} index and sea ice in summer (July-August-September, e.g. Su et al., 2022; Xiao et al., 2015) or autumn (October-November-December, e.g. Kolling et al., 2020). In another study, a longer calibration interval spanning the full sea ice retreat period (March-September) similarly produced statistically significant results (Stoynova et al., 2013). The proxy seasonality therefore remains poorly diagnosed.

In reality, the seasonal bias in the $\ln(PIP_{25})$ index is expected to vary with location as the timing of algal blooms is determined by numerous factors, most notably light intensity and nutrient availability (e.g. Leu et al., 2015; Oziel et al., 2019), and thus is asynchronous across the Arctic (e.g. Ji et al., 2013; Leu et al., 2011). The onset of ice melt, dictated by temperature and regional atmosphere-ocean dynamics (e.g. Horvath et al., 2021; Mortin et al., 2016), also differs significantly across latitudes (e.g. Bliss & Anderson, 2018; Markus et al., 2009) (figure 2). The significant delay of these events from one region to another means that the $\ln(PIP_{25})$ indices obtained from different cores likely reflect sea ice conditions for different months of the year.

In order to constrain this spatially varying seasonality, we analyse published IP_{25} fluxes measured in sediment traps across the Arctic by compositing fitted PDFs and the corresponding SIC

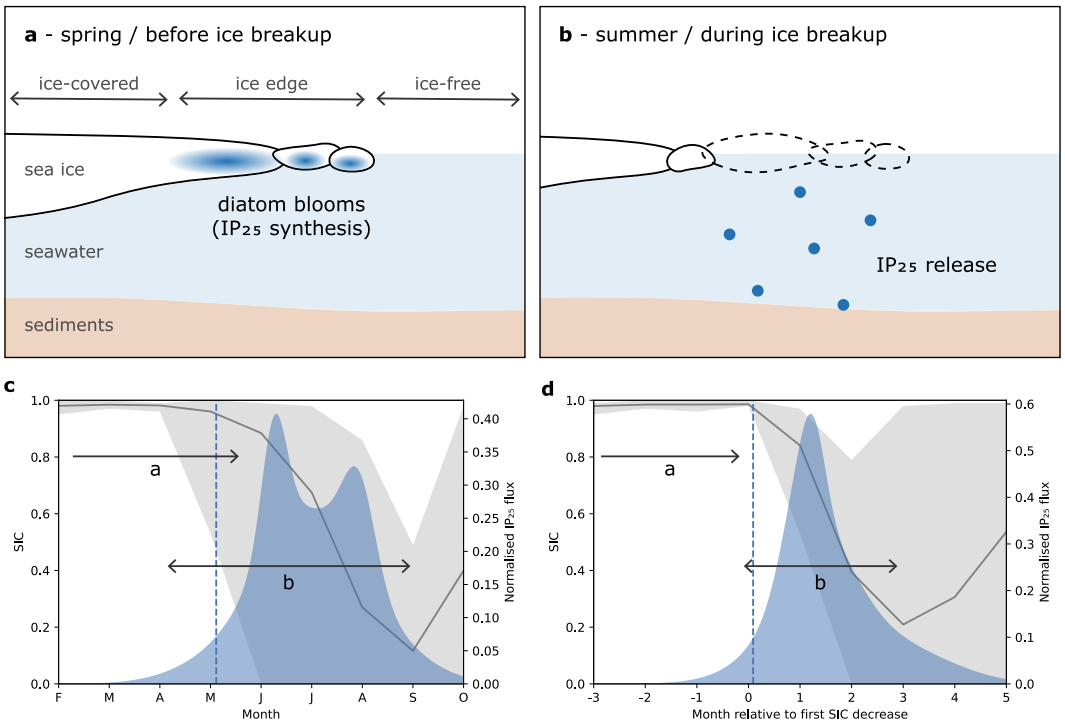

Figure 4. Schematic diagrams of the IP_{25} proxy system (a) in spring / before sea ice breakup and (b) in summer / during sea ice breakup, as well as composite probability density functions (PDFs) of IP_{25} fluxes aligned to (c) calendar months and (d) months relative to the first month of sea ice concentration (SIC) decrease. Dashed line denotes the 5^{th} percentile of the PDF. Shaded area shows the range of SIC observed across all sediment traps, and the trend line represents the error-weighted mean, calculated based on the range of SIC found within a 100 km radius of each trap during the collection period. Arrows indicate the approximate periods corresponding to those illustrated in (a-b).

records (figure 4c). The resultant PDF shows that, on average, IP_{25} release begins in May (>95% confidence), coincident with the average initial sea ice breakup. The highest fluxes occur between June and August, concurrent with the main ice melt period, corroborating a close link between IP_{25} deposition and sea ice thawing. For an Arctic-wide static calibration, the conventional calibration interval of March-April-May (supported by our model; see section 4.2 for details) then corresponds to the three-month interval before IP_{25} release, reflecting IP_{25} production in ice-edge diatom blooms prior to sea ice breakup. This suggests that IP_{25} in the sediments records the maximum SIC before sea ice disintegration, i.e., the $\ln(PIP_{25})$ index is biased towards the time interval immediately prior to local ice melt.

However, the timing of sea ice breakup differs significantly across the trap locations, with an offset of up to three months, and the bimodal distribution of the PDF indicates that fluxes happen in two distinct periods, both supporting a spatially varying seasonal bias. To account for local differences in the timing of ice melt, we align each time series to the month of the first SIC decrease leading to the minimum SIC of the year (figure 4d). The aligned PDF shows that IP_{25} release begins in the same month as initial sea ice breakup (>95% confidence), with the flux peaks synchronised to the following one to two months. The tightened distribution indicates a more precise calibration interval for each sample, which can be determined quantitatively as the three-month interval before the first SIC decrease.

By identifying the proxy seasonality for every individual core, in place of an ambiguously defined "seasonal" bias for the whole Arctic, the spatially varying calibration allows for more accurate and consistent SIC reconstructions across different regions, especially on geologic timescales. While the timing of sea ice breakup at each individual site may have remained largely constant over the accumulation period of the core tops and the sediment traps, it likely differed significantly further back in time under the influence of changing orbital configurations and gateway geometries (e.g. Karami et al., 2021; Timm et al., 2008). It is then unreasonable to assume that a bias to March-April-May SIC persists throughout the reconstruction period.

For illustration of the non-stationarity in proxy seasonality through time, SIC simulations are obtained from the TraCE-21ka dataset, which employs the National Center for Atmospheric Research Community Climate System Model version 3 (NCAR CCSM3) to reconstruct the transient climate evolution over the last 21 ka (Liu et al., 2009). The monthly average ICEFRAC (equivalent to SIC) for the pre-industrial, Mid Holocene, and Last Glacial Maximum experiments are used to derive climatologies, from which the month of the first SIC decrease is calculated. As shown in figure 5, the calendar month in which SIC loss is first observed at any given location shifts with time. Thus, the intimately linked proxy seasonal bias is also expected to change, and the necessity of a varying calibration becomes evident.

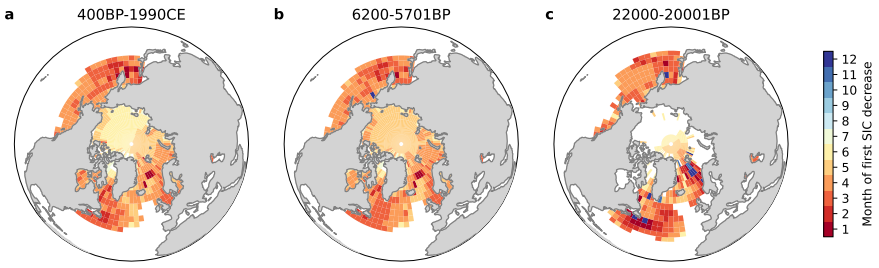

Figure 5. Spatial variations in the timing of the first sea ice concentration (SIC) decrease, derived from the TraCE-21ka experiments for the (a) pre-industrial, (b) Mid Holocene, and (c) Last Glacial Maximum.

3.4 Other Environmental Drivers of ln(PIP_{25})

While sea ice conditions evidently control the timing and spatial distribution of IP_{25} and sterol production, other potential environmental drivers should not be neglected. For example, salinity is known to affect the productivity of sea ice algae (e.g. Glud et al., 2007; Gosselin et al., 1986; Ralph et al., 2007), with laboratory culture experiments showing that sea ice diatom growth decreases with reduced salinity (Grant & Horner, 1976; Søgaard et al., 2011; Zhang et al., 1999). Hyposaline conditions caused by freshwater discharge from large rivers have been implicated in progressively lower IP_{25} concentrations measured near estuaries in the Kara and Laptev Seas (Xiao et al., 2013) and a fjord in Northeast Greenland (Belt, 2018; Ribeiro et al., 2017). Based on ratios between IP_{25} and C_{25}-HBI diene, Xiao et al. (2013) suggested that saturation in HBIs may decrease with lower sea surface salinity (SSS), but research on IP_{25} sensitivity to salinity remains limited. A subsequent study by Limoges et al. (2018) found an increase in the abundance of IP_{25} producers with a slight decrease in bottom sea ice salinity, but did not preclude negative impacts of low salinity on IP_{25} synthesis.

In our dataset, a number of outlying samples with low ln(PIP_{25}) values and high corresponding SIC originate from locations with low SSS values of < 7 g kg^{-1} (figure 3b). When analysing ln(PIP_{25}) with SSS, we find suggestions of a logarithmic relationship between the two under ice-covered conditions, with ln(PIP_{25}) decreasing exponentially as SSS lowers (figure 6a). In such cases, SSS appears to overtake SIC as the limiting factor for IP_{25} production, hindering direct interpretation of sea ice conditions from ln(PIP_{25}) values. As SSS rises to normal levels, this trend disappears and is replaced by a strong negative correlation between ln(PIP_{25}) and SSS, likely an expression of the co-variation between SSS and SIC. As relatively sparse data exist for hyposaline settings, further research is needed to establish a robust relationship between SSS and ln(PIP_{25}).

To disentangle the influence of low SSS on ln(PIP_{25}) from that of SIC in our calibration, we conduct change point analyses on the dataset sorted by SSS using the *ruptures* package (Truong et al., 2020) (see figure S4 for details). The change point is interpreted as a threshold below which SSS overshadows SIC as the dominant predictor of ln(PIP_{25}). For an Arctic-wide calibration to March-April-May, the change point occurs at SSS ~ 21.74 g kg^{-1} for both P_DIP_{25} and P_BIP_{25}. For a spatially varying calibration to the three-month interval before the first SIC decrease, the threshold is detected at SSS ~ 21.26 g kg^{-1}.

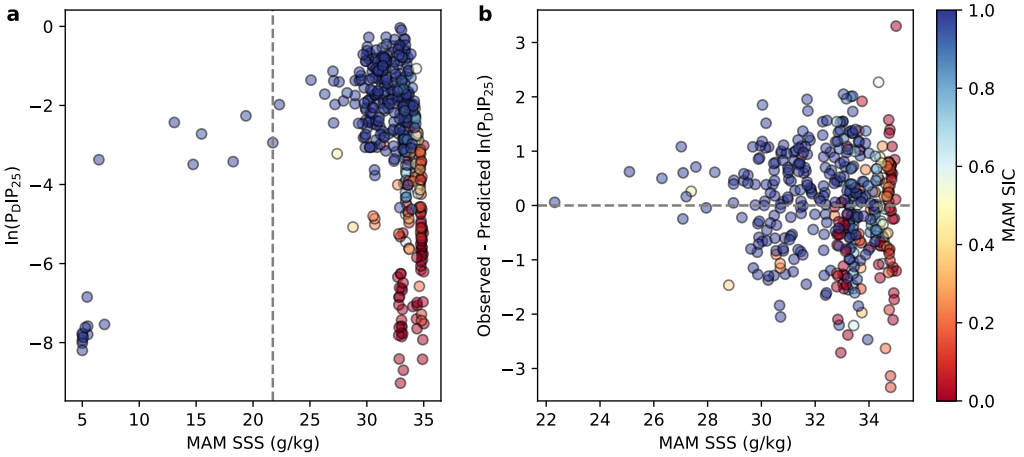

Figure 6. (a) Mar-Apr-May sea surface salinity (SSS) vs. ln(P_DIP_{25}), with dashed line indicating change point (SSS ~ 21.74). (b) SSS vs. model residuals. Colours denote sea ice concentration (SIC).

More generally, as summarised by Belt and Müller (2013), sympagic algal blooms are influenced by a range of factors, including nutrient supply in the water column (e.g. Arrigo et al., 2010; Gradinger, 2009; Leu et al., 2015; Oziel et al., 2019; Rózańska et al., 2009), light availability (which is in turn regulated by the thicknesses of the ice and snow cover; e.g. Arrigo et al., 2010; Leu et al., 2015; Mundy et al., 2005; Oziel et al., 2019), and bottom ice melt rate (Castellani et al., 2017; Lavoie et al., 2005). Their effects on the production of IP_{25} specifically, however, have not been studied in detail. Furthermore, as normalisation by phytoplankton-derived sterols in the ln(PIP_{25}) index negates, to a certain extent, the effects of nutrient levels and light intensity on biomarker synthesis (Müller et al., 2011; Stoynova et al., 2013), and considering that sea surface temperature co-varies with SIC, the sensitivity of ln(PIP_{25}) to these variables is likely low. We therefore leave the identification of additional environmental predictors and their incorporation into the ln(PIP_{25}) calibration for future work.

4 Bayesian Calibration Model

4.1 Model Design

A Bayesian proxy system model (*BaySIC*) is developed to relate ln(PIP_{25}) to SIC based on core-top observations. Since the calibration is based on the spatial relationship between ln(PIP_{25}) and its environmental drivers, and is applied to predict temporal changes in these values, the model assumes ergodicity (Tierney & Tingley, 2014), i.e., the response of the proxy to different environments across space is taken to represent its response to environmental changes over time.

To account for the nonlinear relationship between ln(PIP_{25}) and SIC, as well as to respect the inherent limit of SIC between 0 and 1, the core-top data may be described with a logistic function:

$$\mathrm{SIC} = \frac{1}{1 + \exp -(\beta_0 + \beta_1 \ln(\mathrm{PIP}_{25}))}, \tag{3}$$

where SIC and ln(PIP_{25}) are vectors representing the core-top data, β_0 is the intercept, and β_1 is the slope. However, a regression model in this form considers SIC as a function of ln(PIP_{25}), which contradicts the natural causal relationship between the proxy and its environmental predictors. In nature, SIC serves as the predictor variable for ln(PIP_{25}). Assuming that the prediction errors are normally distributed, the relationship can be expressed as follows:

$$\ln(\mathrm{PIP}_{25i}) \mid \beta_0, \beta_1, \phi \sim \mathcal{N}(g(\mathrm{SIC}_i), \phi), \tag{4}$$

where PIP_{25i} denotes the core-top sample, SIC_i denotes the corresponding SIC data, $g(x) = \frac{-\ln(\frac{1}{x}-1)-\beta_0}{\beta_1}$ is the inverse of equation 3, and ϕ is the variance, which is introduced by uncertainties in the SIC observations. Thus, we obtain the forward model in the following form:

$$\ln(\mathrm{PIP}_{25i}) = \frac{-\ln(\frac{1}{\mathrm{SIC}_i} - 1) - \beta_0}{\beta_1} + \epsilon_i, \tag{5}$$

$$\epsilon_i \sim \mathcal{N}(0, \phi), \tag{6}$$

where ϵ_i represents the residual error associated with each sample. The inverse logistic function (equation 5) has a domain of (0, 1), which allows the transformation of SIC data within the same range. As SIC approaches 0, ln(PIP_{25}) decreases exponentially; as SIC approaches 1, ln(PIP_{25}) increases exponentially.

The model parameters (β_0, β_1, and ϕ) are inferred using a Bayesian framework. Instead of a single estimate for each parameter, Bayesian analyses yield probability distributions (posteriors), which serve to quantify the uncertainties of model predictions. The posteriors are derived from (*i*) the priors, which are assigned to reflect the current scientific understanding of the parameters, and (*ii*) the likelihood, which is computed from the data given the parameters. Therefore, the posteriors represent updated beliefs of the parameters that are informed by the data, which, in our case, consist of the core-top ln(PIP_{25}) values and their corresponding satellite SIC observations. Accordingly, their spread reflects uncertainties in both the data and the calibration.

To the best of our knowledge, there exists no published nonlinear calibration for $\ln(PIP_{25})$ that can provide a basis for prior expectations for the regression coefficients. Hence, uninformative priors are used such that the posteriors are predominantly influenced by the data. The normal distribution is chosen for its real-valued, unbounded domain (i.e., $\beta \in \mathbb{R}$), and is centred around 0 so as not to favour positive or negative values a priori. For variance, a prior constrained to positive real numbers is required (i.e., $\phi \in \mathbb{R}^+$); the inverse gamma distribution is conventionally employed in Bayesian models for this purpose. The distributions are defined as follows:

$$\beta_0 \sim \mathcal{N}(0, 3), \tag{7}$$

$$\beta_1 \sim \mathcal{N}(0, 3), \tag{8}$$

$$\phi \sim \mathcal{IG}(2, 0.5); \tag{9}$$

Using larger prior standard deviations in sensitivity tests does not result in significant changes in the posteriors, indicating that the model is robust to the choice of priors.

Since our 22-year SIC dataset constitutes only a fraction of the time represented in most samples, and its grids do not perfectly match the areas integrated by the core tops, we further treat the SIC corresponding to each ln(PIP) as an unknown. ~~T~~Under the Bayesian framework, the distribution associated with each SIC parameter thus simulates the year-to-year sea ice variability over the (unknown) time and area integrated by the core top.

The prior for each SIC parameter is defined by a beta distribution, chosen for its flexibility to accommodate vastly different distributions within the fixed limits of 0 and 1, as follows:

$$\mathrm{SIC}_i \sim \mathcal{B}eta(\alpha_i, \beta_i), \tag{10}$$

$$\alpha_i = \frac{\mu_i}{IQR_i}, \tag{11}$$

$$\beta_i = \frac{1}{IQR_i} - \alpha_i, \tag{12}$$

where μ and IQR are the mean and interquartile range of the 1979-2000 SIC dataset, respectively. This centres the prior distribution on the mean with a variance proportional to the IQR, effectively assigning smaller regression weights to samples with higher SIC variability. The Kullback–Leibler divergence, a measure of the difference between probability distributions (Kullback & Leibler, 1951), is small across all SIC parameters, indicating that the simulated distributions provide good approximations of the empirical distributions (figures S5 and S6). SIC values of zero are assumed to be under the satellite detection limit and are replaced by the minimum non-zero SIC value in the dataset.

In the forward model, the spatially varying seasonal bias in $\ln(PIP_{25})$ is addressed by matching each core-top sample with the climatological mean SIC of the calibration interval deduced from sediment trap studies, i.e., the three months before the first SIC decrease (figure 4d). This means that model-estimated SIC values for different months will be used to infer $\ln(PIP_{25})$ values at different locations. For example, in high latitude regions where sea ice breakup does not begin until July, the calibration interval will be May-June-July. As the timing of sea ice retreat changes through time, the model also accommodates temporal changes in proxy seasonality, facilitating its application in geologic time. The month of the first SIC decrease at a given location is determined by rounding the monthly climatologies to the nearest 0.05 and finding the month of the maximum SIC leading to the minimum. This requires seasonally varying SIC and fails where SIC remains constant throughout the year, such as locations that are always ice-free or ice-covered. For these cases, the month of the first SIC decrease is taken from the nearest grid with variable SIC, assuming that any IP_{25} deposition occurs either by lateral transport or during sea ice thinning which would be concurrent with nearby SIC decrease.

The likelihood is then calculated by:

$$\mathcal{L}(\ln(\mathrm{PIP}_{25}) \mid \beta_0, \beta_1, \phi, \mathrm{SIC}) = \prod_{i=1}^{n} P(\ln(\mathrm{PIP}_{25i}) \mid \beta_0, \beta_1, \phi, \mathrm{SIC}_i), \tag{13}$$

[Modified from $\mathcal{L}(\beta_0, \beta_1, \phi, \text{SIC} \mid \ln(\text{PIP}_{25})) = \prod_{i=1}^{n} f(\ln(\text{PIP}_{25i}) \mid \beta_0, \beta_1, \phi, \text{SIC}_i)$,] where n is the total number of core tops, and $P(\cdot)$ is used to denote PDFs.

By Bayes' Theorem, the following proportionality may be obtained:

$$P(\beta_0, \beta_1, \phi, \text{SIC} \mid \ln(\text{PIP}_{25})) \propto \mathcal{L}(\ln(\text{PIP}_{25}) \mid \beta_0, \beta_1, \phi, \text{SIC})\ P(\beta_0, \beta_1, \phi, \text{SIC}), \tag{14}$$

[Modified from $f(\beta_0, \beta_1, \phi, \text{SIC} \mid \ln(\text{PIP}_{25})) \propto \mathcal{L}(\beta_0, \beta_1, \phi, \text{SIC} \mid \ln(\text{PIP}_{25}))\ f(\beta_0, \beta_1, \phi, \text{SIC})$,] where ~~$f$~~$P(\beta_0, \beta_1, \phi, \text{SIC})$ is the product of all the prior distributions, with the assumption that the parameters are independent of one another. Given the large number (~~> 400~~$n + 3$) of parameters, we use the *t-walk* (Christen & Fox, 2010), a Markov chain Monte Carlo sampler to infer the posteriors for all parameters. The ensemble of parameters obtained, representing possible calibration curves given the data, can then be used to calculate the predictive distribution, which integrates over model uncertainties and provides a probabilistic estimate of $\ln(\text{PIP}_{25})$ given any SIC value.

Based on change point analyses (Truong et al., 2020), we exclude samples with low SSS in our calibration to focus on the relationship between SIC and $\ln(\text{PIP}_{25})$. Therefore, the model can only predict $\ln(\text{PIP}_{25})$ from SIC when and where SSS meets the determined threshold, which differs slightly depending on the calibration interval. Should the proposed logarithmic relationship between SSS and $\ln(\text{PIP}_{25})$ be independently verified in the future, we suggest a pre-treatment of samples from hyposaline settings to correct for the additional influence.

Since the logit function describes a one-to-one relationship between SIC and $\ln(\text{PIP}_{25})$, the forward model can be inverted to estimate past SIC directly from downcore $\ln(\text{PIP}_{25})$ values (equation 3). Through Bayesian inference, the same ensemble of parameters is used to propagate calibration uncertainties into the predictions. However, as the timing of the first SIC decrease is unknown in the inverse case, a spatiotemporally stationary proxy seasonality must be assumed. We experiment with different calibration intervals to determine the optimum interval for such an Arctic-wide static calibration. Results from the inverse model should also be analysed with salinity data wherever possible; if SSS is below the detected threshold for the calibration, the model may be prone to underestimate SIC.

4.2 Model Results

The *BaySIC* model and its residuals are shown in figure 7, and its metrics in table 1. The relationship between SIC and $\ln(\text{PIP}_{25})$ is well described by the inverse logistic function. The spatially varying calibration explains 74% of the variance in the $\ln(\text{P}_\text{D}\text{IP}_{25})$ index calculated with our core-top biomarker database, showing a marked improvement from the previous pan-Arctic calibration (Xiao et al., 2015). The model has a root mean square error of prediction of 0.96, which is reasonable given the spread of the core-top data, particularly in locations with more variable SIC. As these samples are down-weighted in the regression, the calibration curve is largely determined by data points with SIC close to 0 or 1. In general, there exists no strong spatial pattern in the residuals, supporting model application across the Arctic. This is not the case in sensitivity tests that include samples from Stoynova et al. (2013) and Su et al. (2022) (figure S7), further justifying their exclusion from our calibration database.

The posteriors for the regression coefficients have significantly smaller spreads than the priors (figure S8), indicating the dominance of the likelihood function, i.e., the intercept and slope of the model are mostly informed by the core-top data. Similar results are obtained using the full satellite SIC record (1979-2022) or historical datasets (1950-2000 and 1950-2017) to inform the priors (see table S2 for details), further supporting the model's robustness to different temporal frameworks. The posterior for variance shows an increase from the prior, reflecting data constraints on the precision of the model.

~~The 95% highest density interval (HDI) spans approximately 3 $\ln(\text{PIP}_{25})$ units, which represent quantified uncertainties in both the observations and the calibration.~~Uncertainties in both the observations and the calibration can be quantified using the 95% highest density interval (HDI), which is the smallest

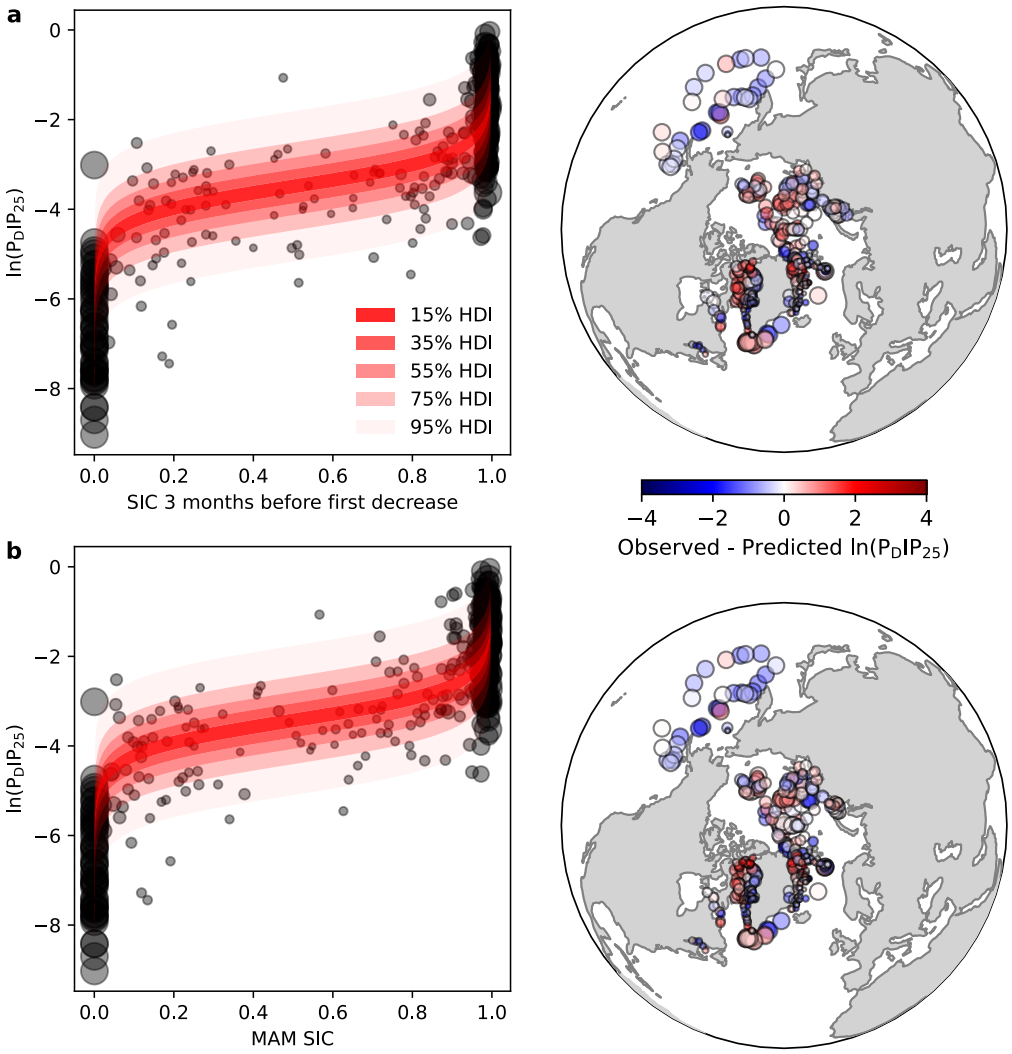

Figure 7. Calibrations (left) for $\ln(P_DIP_{25})$ using the sea ice concentrations (SIC) of (a) the average of the three months before the first SIC decrease and (b) Mar-Apr-May, and the corresponding spatial distributions of residuals (right). Bubble size is inversely proportional to the interquartile range of the SIC over the 22-year calibration period. HDI = highest density interval.

Table 1. Calibration results of different $\ln(PIP_{25})$ indices to the sea ice concentration (SIC) of different months (e.g. MAM = Mar-Apr-May). RMSEP = root mean squared error of prediction.

	3 months before first SIC decrease	MAM	AMJ	Apr	May
$\ln(P_DIP_{25})$					
R^2	0.74	0.74	0.72	0.73	0.70
RMSEP	0.96	0.96	1.01	0.99	1.04
$\ln(P_BIP_{25})$					
R^2	0.63	0.63	0.59	0.63	0.57
RMSEP	1.47	1.48	1.54	1.47	1.58
SSS threshold	21.26	21.74	21.45	23.05	21.61

region that contains 95% of the posterior distribution, representing the most credible values. In this calibration, the 95% HDI spans approximately 3 ln(PIP_{25}) units. Since the inverse logistic function is characterised by a gently-sloped body between steeply-sloped tails, the *BaySIC* model is more sensitive to extreme than intermediate SIC values. This means that in the inverse framing, where downcore ln(PIP_{25}) are used to reconstruct SIC, the uncertainties associated with extreme ln(PIP_{25}) values will be smaller than those associated with intermediate ln(PIP_{25}) values (see section 5 for illustrated examples). As the core-top data show that ln(PIP_{25}) ~ -4 can result from the full range of SIC, SIC reconstructions from these values are highly uncertain and should be interpreted with caution. Away from this step-like transition, the model can distinguish between ice-free and ice-covered conditions with relatively high certainty. Moreover, within the existing core-top database, there is a ~ 1:4 imbalance of paired IP_{25}-sterol data collected from seasonally ice-free (SIC ~ 0) versus seasonally ice-covered (SIC ~ 1) locations (figure 7). Increasing data coverage near the seasonally ice-free transition would provide more constraints on the lower end of the slope.

Following the removal of core tops matched with low SSS, no significant trend is observed between SSS and the residuals among the remaining samples (figure 6b). Since the influence of salinity on ln(PIP_{25}) is only apparent at anomalously low SSS levels, the filtering procedure is deemed more suitable than the addition of a second predictor in the calibration model. Analyses with SST and nutrient data similarly show no correlation between the residuals and these environmental variables (figure S9), suggesting that they are not major drivers of ln(PIP_{25}). Future work is needed to identify the source(s) of the variance left unexplained by *BaySIC*.

Similar calibration curves are obtained for ln(P_BIP_{25}), but some structures in the spatial distribution of residuals are discernible (see Appendix A). In particular, strong negative residuals exist to the northeast of Svalbard, where low ln(P_BIP_{25}) values are associated with ice-covered conditions (and normal SSS levels). As Belt et al. (2015) pointed out in their original study, additional brassicasterol may be contributed by non-pelagic sources, which would explain the lower-than-expected IP_{25}-brassicasterol ratios. However, as these core tops lack corresponding dinosterol measurements, it is possible that their ln(P_DIP_{25}) values are equally low, which would point to other causes of discrepancy. *BaySIC* incorporates this unknown source of uncertainty by taking into account these anomalous samples and converging to a higher variance. Thus, the ln(P_BIP_{25}) calibration has a greater uncertainty range that reflects potential additional influences on the proxy (see examples below).

For an Arctic-wide static calibration, March-April-May appears to be the optimum calibration interval, with an alternative calibration to April-May-June yielding similar results. This is consistent with previous calibrations and corroborates the interpretation that ln(PIP_{25}) reflects SIC shortly before sea ice breakup (discussed in section 3.3). Although this model performs similarly to the spatially varying model in replicating core-top samples, we argue that the consideration of a variable proxy seasonality remains important for accurate predictions. By identifying ln(PIP_{25}) as recording the maximum SIC before sea ice disintegration, the model outputs for the corresponding months may be used to reconstruct the maximum sea ice extent, rather than the average sea ice conditions over a loosely defined Arctic spring.

To test this hypothesis and to evaluate model performance, we apply *BaySIC* to out-of-sample SIC observations from locations with paired IP_{25}-sterol sediment trap data. The average SIC of the three months before the first SIC decrease during the sampling period are supplied to the model to generate probabilistic ln(PIP_{25}) estimates. For the traps at ~ 75° latitude (Gal et al., 2022), this interval is March-April-May. For those at ~ 83° latitude (Nöthig et al., 2020), it is April-May-June. The results are compared against the observed ln(PIP_{25}) values, which are calculated using the total biomarker fluxes measured over the sampling period. Overall, there is good agreement between the *BaySIC* predictions and sediment trap data, with the observations always falling within the 95% HDI (figure 8). The maximum a posteriori (MAP) estimation, representing the mode of the predictive distribution, converges closely with the observation.

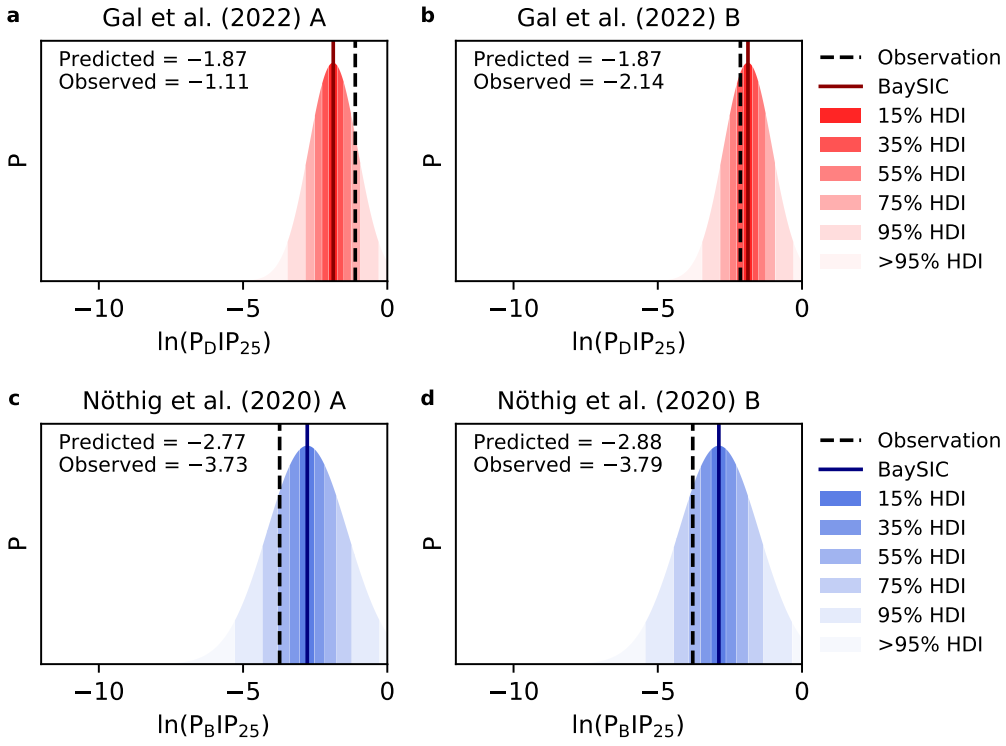

Figure 8. Predictions of the spatially varying forward model vs. observations from sediment traps of (a-b) $\ln(P_DIP_{25})$ and (c-d) $\ln(P_BIP_{25})$. Trap locations are shown in figure 2. HDI = highest density interval.

We repeat the exercise using the Arctic-wide static March-April-May calibration to assess the potential impacts of assuming stationary proxy seasonality. For the two traps located at a higher latitude, this results in a one-month offset from the seasonal bias diagnosed by the spatially varying model. In both cases, the prediction deviates further from the observation than that obtained above by ~ 0.11 ln(PIP_{25}) units (not shown). This supports our hypothesis that the consideration of a dynamic proxy seasonality yields more accurate forward modelling results and, despite relatively small differences derived here from modern observations, is consequential in deep-time applications (discussed in section 3.3).

5 Palaeoclimate Applications

5.1 Quantitative SIC Reconstruction from Downcore Biomarker Measurements

By establishing a fully quantitative relationship between SIC and the new ln(PIP_{25}) index, *BaySIC* overcomes the longstanding limitation to semi-quantitative SIC reconstruction of the original PIP_{25} index. To exemplify its palaeoclimate applications, we apply *BaySIC* to a sediment core in northeastern Fram Strait (MSM5/5-712-2; 78°54.94'N, 6°46.04'E; 1487 m; Budéus, 2007) that has been analysed for both biomarkers and dinoflagellate cyst (dinocyst) assemblages. The published IP_{25} and sterol measurements (Cabedo-Sanz & Belt, 2016; Müller & Stein, 2014; Müller et al., 2012) are placed on the same chronology as the palynological data (Falardeau et al., 2019) to permit comparisons between the records, which extend into the Last Glacial Maximum (LGM; 23 ka).

Paired IP_{25}-dinosterol and IP_{25}-brassicasterol measurements are supplied to the inverse model to estimate past SIC from ln(P_DIP_{25}) and ln(P_BIP_{25}), respectively. Within *BaySIC*, all biomarker measurements are treated with the best estimate of the detection limit prior to calculating the ln(PIP_{25}) index (discussed in section 3.1). Based on reconstructions presented by Falardeau et al. (2018), SSS at the core site fluctuated between 24 and 36 psu in the last 23 ka, remaining well above the determined threshold (table 1). Thus, salinity is assumed to have negligible influence on the biomarker records presented here.

Overall, the SIC reconstructions using either index show good agreement with each other (figure 9a-b). For the LGM, both indices reconstruct near-complete ice cover, with amplified SIC fluctuations in the ln(P_DIP_{25}) reconstruction. Partial ice cover persisted during Heinrich event 1 and the Bølling-Allerød, but higher SICs are reconstructed from ln(P_BIP_{25}) in several intervals. These discrepancies are due to differences in the IP_{25}-sterol ratios and are also found in reconstructions using the original PIP_{25} index (see section 5.2). Near-identical trends are obtained for the Younger Dryas (YD) and throughout most of the Holocene, only diverging in the last 2 ka. The inconsistencies here are due to the integration of the Cabedo-Sanz and Belt (2016) dataset, which reports lower IP_{25} concentrations than (and similar brassicasterol concentrations as) measurements at the same depths provided by Müller et al. (2012), and does not include data for dinosterol. Near the top of the core, rapid sea ice loss is inferred from both indices and the reconstructions converge towards the modern March-April-May SIC observed at the core site.

The 95% HDI for both reconstructions are large (given site MSM5/5-712-2's location near the MIZ), but realistic considering the various sources of uncertainty incorporated. As explained in the previous section, the uncertainty ranges associated with extreme ln(PIP_{25}) values are smaller, for example, during the YD when the proxy strongly indicates ice-covered conditions. In addition, reconstructions based on ln(P_DIP_{25}) feature less uncertainty than those derived from ln(P_BIP_{25}), which reflects higher confidence in its correlation with SIC in the core-top calibration.

5.2 Comparison with Prior SIC Reconstruction Approaches

To illustrate the differences in SIC reconstruction via ln(PIP_{25}) and the original PIP_{25} index, we apply previous linear calibrations for the region of East Greenland and West Spitsbergen (Müller et al., 2011) to the same biomarker data. As the core was divided into sections and

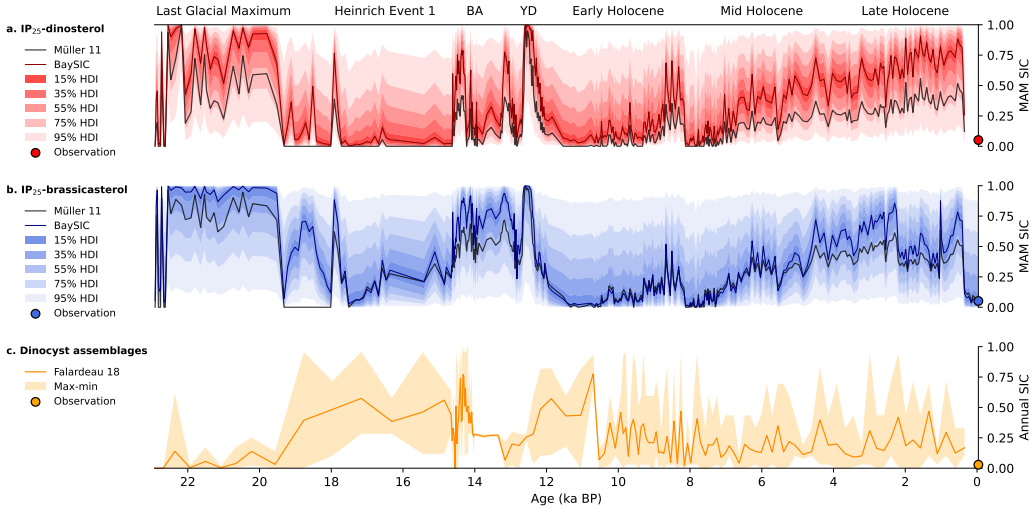

Figure 9. Reconstructions of Mar-Apr-May sea ice concentration (SIC) at site MSM5/5-712-2 based on paired (a) IP_{25}-dinosterol and (b) IP_{25}-brassicasterol measurements (Cabedo-Sanz & Belt, 2016; Müller & Stein, 2014; Müller et al., 2012), using the *BaySIC* inverse model and the regional linear calibrations presented by Müller et al. (2011). HDI = highest density interval. (c) Reconstruction of annual SIC at the same site via dinocyst assemblages from Falardeau et al. (2018). Circles denote modern (1979-2000) SIC observed at the core site. ~~Grey shading indicates cold intervals.~~ YD = Younger Dryas; BA = Bølling-Allerød.

analysed separately, different *c* factors were employed in the calculation of PIP_{25} by each study (Cabedo-Sanz & Belt, 2016; Müller & Stein, 2014; Müller et al., 2012). In order to use the published calibrations, we recalculate the P_DIP_{25} and P_BIP_{25} values based on the *c* factors derived by Müller et al. (2011). The highly variable and somewhat arbitrarily defined *c* factor is an inherent limitation of the original PIP_{25} index approach; by eliminating it from $\ln(PIP_{25})$, *BaySIC* enables consistent proxy interpretation over space and time. Its applicability across the Arctic further removes the need for a regional calibration, allowing quantitative proxy interpretation in locations where it was previously not possible.

Unlike *BaySIC*, the linear regression model takes SIC beyond 0 and 1 at extreme PIP_{25} values; we place additional limits on the reconstructions to restrict them to the natural range of the parameter. In general, *BaySIC* predictions are consistent with the results of the adapted PIP_{25} index approach (figure 9a-b), which reflects the common biomarker data used for both indices. *BaySIC* tends to estimate greater magnitude SIC changes than the linear regression model, for instance, the rapid decrease from full ice cover at the end of the LGM. Similarly, the reconstructions diverge from Mid Holocene onwards, with *BaySIC* suggesting near-complete ice cover in contrast to the partial ice cover indicated by the linear calibration model. This is an expression of the demonstrated nonlinearity of the proxy: at the transition between ice-covered and ice-free conditions, *BaySIC* captures small shifts in $\ln(PIP_{25})$ and deduces relatively large SIC changes.

Between 18 and 19 ka, completely ice-free conditions are reconstructed from the original PIP_{25} indices, whereas *BaySIC* estimates partial ice cover. These inconsistencies arise from the zero IP_{25} concentrations measured for the sediment samples, leading to zero PIP_{25} values indicative of open ocean conditions. However, based on the low corresponding sterol concentrations, Müller and Stein (2014) concluded that the biomarkers record permanent ice cover instead. This has conventionally been handled by designating a PIP_{25} value of 1 to samples with IP_{25} and sterol concentrations under or near their limit of detection (Belt, 2018). *BaySIC* results show that once the biomarker measurements are treated with the detection limit, they can be readily related to

the full range of SIC via the ln(PIP_{25}) index (section 4.2), suggesting that the relative biomarker abundances remain informative even when absolute abundances are low. As reported IP_{25} and sterol concentrations both tend to 0, ln(PIP_{25}) approaches −2.35 to −3.06, depending on the sterol and the unit of measurement used. According to the calibrations, these values would indicate mostly ice-covered conditions, in agreement with previous interpretations of the proxy system. As biomarker concentrations increase, their ratio becomes less sensitive to the added minimum concentrations. The *BaySIC* approach maintains the separation between observation and interpretation to avoid introducing additional bias into SIC reconstructions.

Despite similarities in the reconstructions, the major breakthrough made by *BaySIC* lies in its fully quantitative proxy interpretation. Owing to challenges in quantifying the original PIP_{25} index, it has traditionally been used to reconstruct sea ice only semi-quantitatively by categorising sea ice conditions and matching each to a range of index values. In their original ~~study~~reconstruction, Müller et al. (2012) distinguish between extended, marginal, and variable/less ice cover, as well as ice-free conditions, instead of deriving SIC from the PIP_{25} index as attempted here. With *BaySIC*, ln(PIP_{25}) is mapped to the full, continuous range of SIC, clarifying the proxy interpretation and facilitating direct comparison with model outputs. Its Bayesian framework further quantifies the uncertainties, which have been lacking in previous linear calibrations for PIP_{25}. The resultant probabilistic estimates may help reconcile different proxy records and achieve more robust palaeoclimate reconstructions.

As an example, we compare *BaySIC* results against an independent sea ice reconstruction using dinocyst assemblages (Falardeau et al., 2018). The reconstruction is converted from ice-covered months per year, where ice cover is defined as SIC > 0.5, to annual SIC (figure 9c); a good correlation has previously been shown between the two variables (de Vernal, Rochon, et al., 2013). The average SIC reconstructions are therefore expected to be lower and less variable than those from ln(PIP_{25}) and PIP_{25}, which are seasonally biased. A detailed analysis of the record is presented in the original study; here, we highlight several key differences between the proxy reconstructions.

During the LGM, persistent ice cover is reconstructed from ln(PIP_{25}), followed by a rapid transition to mostly ice-free conditions at 19 ka. An opposite trend is shown by dinocyst assemblages, which suggest little to no ice cover throughout the LGM, succeeded by partial ice cover. The contradiction is likely due to limitations of the modern analogue technique employed in quantitative sea ice reconstruction from dinocyst assemblages: as Falardeau et al. (2018) pointed out, the best matches found for their LGM samples were from a location that experienced distinct hydrographical conditions to those expected for the core site. Without suitable modern equivalents, the resultant SIC reconstructions may be inaccurate. In contrast, the diverse settings in which IP_{25} and the sterols have been detected and the clear relationship between the ln(PIP_{25}) index and SIC renders the proxy applicable in different palaeo-environments.

Both proxies record a relatively short-lived SIC increase at 14 ka, followed by partial ice cover during the Bølling-Allerød. Evidence of the YD cooling is similarly clear in all reconstructions, with the ln(PIP_{25}) indices indicating a sharper SIC rise to completely ice-covered conditions, compared to a slower and more modest increase shown by dinocyst assemblages. The elevated SIC persisting into Early Holocene registered by the dinocyst assemblages is not discernible in ln(PIP_{25}) reconstructions. From Mid to Late Holocene, the reconstructions further diverge: a steady SIC increase is reconstructed via ln(PIP_{25}), following the decline in the orbital forcing in the Northern Hemisphere, while the dinocyst assemblages suggest relatively stable, low annual SIC. As ln(PIP_{25}) tracks the maximum SIC, sea ice changes in seasonally ice-covered locations are more readily observable, providing more precise insights into past sea ice conditions.

5.3 Sea Ice in Past Warm Periods

The new calibrations offer opportunities to reevaluate available proxy records for probabilistic insights into Arctic sea ice responses to past warming. For additional examples, we apply *BaySIC* to sites with paired IP_{25}-sterol measurements dated to the Last Interglacial (LIG, ~

130 − 118 ka) and the mid-Pliocene Warm Period (mPWP, ~ 3.3 − 3.0 Ma). These data have previously been interpreted either qualitatively or semi-quantitatively (summarised in table 2). In the absence of reliable salinity data for each site and period, we ignore, for illustrative purposes, the possibility of drastic SSS changes. The published biomarker concentrations (Clotten et al., 2017; Knies et al., 2014; Kremer et al., 2018; Stein et al., 2017, 2018; Steinsland et al., 2023) are averaged over the target interval as inputs for the inverse model, yielding a non-Gaussian PDF for each SIC reconstruction (figure 10). This means that the HDIs are not centred at the MAP estimation, i.e., there is a higher probability for SIC to fall closer to one end of the spectrum (also seen in figure 9), and reflects that most of the ocean is either ice-covered or ice-free, such that the chances of the core site being within the MIZ is relatively low.

Table 2. Previous interpretation of sea ice conditions during the mid-Pliocene Warm Period (mPWP) or the Last Interglacial (LIG) at each site. Core locations are shown in figure 10.

Core	Previous sea ice interpretation	Study
mPWP		
ODP910C	Similar to the modern summer minimum	Knies et al. (2014)
ODP151-907A	Ice-covered in spring, ice-free in summer	Clotten et al. (2018)
LIG		
PS2200-5	Perennial ice cover	Stein et al. (2017)
PS2138-2	Spring/summer SIC of ~ 20% or less	Stein et al. (2017)
PS92/039-2	Perennial ice cover	Kremer, Stein, Fahl, Ji, et al. (2018)
PS93/006-1	Partially ice-covered in summer	Kremer, Stein, Fahl, Bauch, et al. (2018)
GS16-204-22CC-B	Marginal ice zone	Steinsland et al. (2023)

For the LIG, *BaySIC* predicts relatively high (~ 0.7 or more) March-April-May SIC for PS2200-5, PS93/006-1, and GS16-204-22CC-B, supporting the presence of sea ice in spring as formerly inferred for these sites (Kremer, Stein, Fahl, Bauch, et al., 2018; Stein et al., 2017; Steinsland et al., 2023). The tight PDF obtained for PS2200-5 in particular indicates high confidence in the interpreted ice-covered conditions, which is broadly consistent with this site's northerly location. Slightly more sea ice coverage is estimated for GS16-204-22CC-B than in the original study, which considered the biomarkers individually rather than combined in an index. Compared with the traditional approach of classifying sea ice conditions, with categories like the MIZ spanning a wide range of SIC, the redefined $\ln(PIP_{25})$ index and its calibration to SIC allow more specific reconstructions.

BaySIC estimates very low (~ 0.1 or less) March-April-May SIC for PS92/039-2, contradicting the previously inferred perennial ice cover (Kremer, Stein, Fahl, Ji, et al., 2018). This disagreement stems from the setting of PIP_{25} to 1 for samples with low IP_{25} and brassicasterol concentrations in the original study, as opposed to the detection limit treatment implemented within *BaySIC* (discussed in section 5.2). By considering the ratios of the biomarkers via $\ln(PIP_{25})$, our model suggests that this site had more likely experienced ice-free conditions during the LIG. For PS2138, the *BaySIC* prediction via $\ln(P_BIP_{25})$ corroborates sea ice conditions deduced from P_BIP_{25} by Stein et al. (2017), but diverges from the much higher SIC predicted via $\ln(P_DIP_{25})$. Further investigation is needed to explain this discrepancy. One potential cause is additional brassicasterol sources (discussed in section 2.1), in which case the local SIC over the LIG would have been previously underestimated. As *BaySIC* provides the full probability distributions for each reconstruction, it is also possible to determine the most probable SIC as indicated by all biomarkers by considering the results obtained via both sterols.

Turning to the mPWP, a similar divergence is observed in predictions for ODP151-907A: the $\ln(P_DIP_{25})$ record strongly indicates SIC to be close to 1, whereas the $\ln(P_BIP_{25})$ record pro-

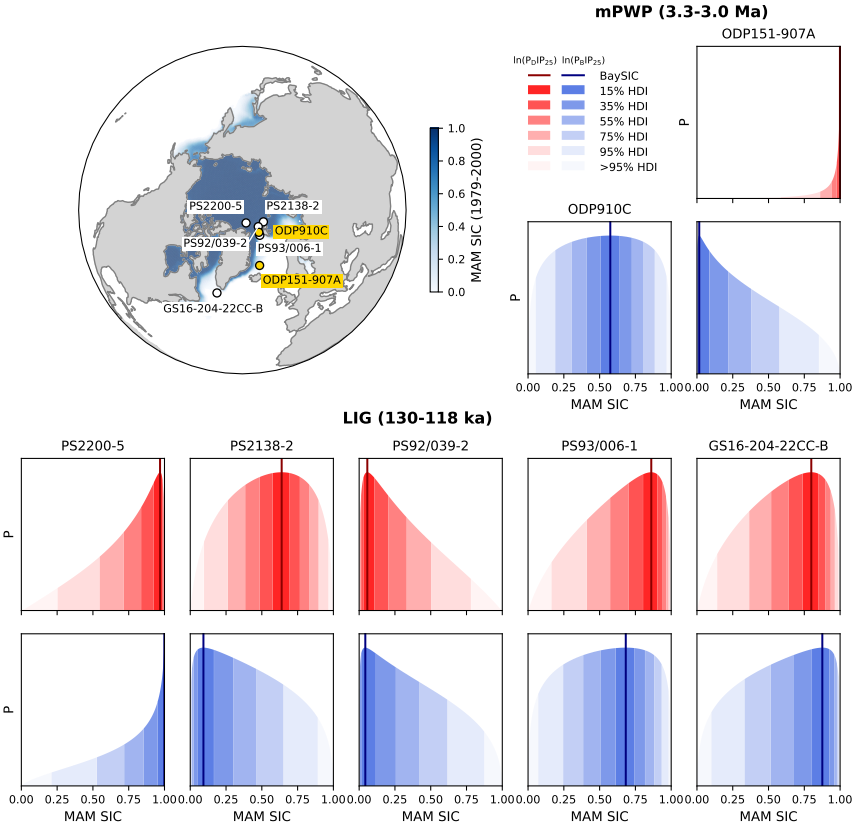

Figure 10. *BaySIC* reconstructions of Mar-Apr-May sea ice concentration (SIC) for seven sites with mid-Pliocene Warm Period (mPWP, yellow) or Last Interglacial (LIG, white) paired IP_{25}-sterol measurements. The map shows their locations and modern (1979-2000) SIC. MAP = maximum a posteriori (estimation); HDI = highest density interval.

vides only weak constraints on SIC. Clotten et al. (2018) attributed the decoupling of the two sterols during this period to non-marine sources of brassicasterol, which would lend more credibility to the fully ice-covered scenario suggested by $\ln(P_DIP_{25})$. The ODP910C site is estimated to be ice-free based on $\ln(P_BIP_{25})$, consistent with the former interpretation (Knies et al., 2014). However, dinosterol data is not available for this core. Given the occasional but significant conflicts between SIC reconstructions employing different sterols, interpretations based on only one of the two should be treated with extra caution.

Direct comparisons of SIC across distant localities and distinct ages, as shown above, have previously proven difficult due to issues pertaining to the *c* factor and regional correlations; *BaySIC* facilitates spatially and temporally consistent sea ice interpretations, bringing a new perspective to ongoing debates about Arctic sea ice extent during past warm periods. While recent studies have inferred seasonally ice-free conditions in the LIG indirectly through summer surface air temperature proxies (Sime et al., 2023), or qualitatively through the presence of an open water proxy (Vermassen et al., 2023), more proxy-based investigations are required to confirm such proposition and to better define sea ice sensitivity to warming. In this regard, *BaySIC* provides a critical step toward achieving direct and quantitative solutions.

6 Conclusions

A new $\ln(PIP_{25})$ index is proposed as a robust Arctic sea ice proxy that enables fully quantitative proxy reconstructions of palaeo-sea ice concentration (SIC). It improves on the established PIP_{25} index by eliminating the use of a problematic balance factor, thus allowing direct comparisons across different Arctic regions and consistent interpretations on longer (geologic) timescales. The $\ln(PIP_{25})$ index is found to correlate nonlinearly with SIC, with an apparent additional influence of low sea surface salinity warranting further investigation. Observations from published sediment trap studies indicate a proxy seasonal bias towards the interval preceding local sea ice breakup, which varies over both space and time.

Using a pan-Arctic core-top biomarker database, we develop a set of Bayesian models, called *BaySIC*, to calibrate the $\ln(PIP_{25})$ index to seasonal SIC. Calibration uncertainties are quantified and propagated to model predictions, providing better constraints on model uncertainties. The spatially varying forward model considers differences in the timing of ice melt, yielding more accurate proxy predictions while facilitating proxy-model comparisons and palaeoclimate data assimilation. An inverse model is also devised, by assuming an Arctic-wide stationary bias to March-April-May, to support direct SIC reconstructions from downcore $\ln(PIP_{25})$ measurements. Finally, we provide a number of examples that demonstrate the applicability of *BaySIC* to palaeoclimate investigations, which highlight the advances made in sea ice reconstruction using IP_{25} and open-water sterols.

As the first model of its kind, *BaySIC* represents an important step in translating the now well-established sea ice proxy into a quantified climate variable, opening up new possibilities for its use in constraining the long-term variability of Arctic sea ice, thereby improving our understanding of past and future climate changes. Future research may provide more insights into the proxy system, including the identification of other environmental factors affecting $\ln(PIP_{25})$, which may help explain the remaining variance in the index. Additional core-top biomarker datasets, especially from currently under-sampled Arctic and sub-Arctic regions, may further strengthen the constraints on the calibration curves and their associated uncertainty ranges, enabling more robust sea ice, and thus global climate, reconstructions.

Appendix A Model results for $\ln(P_BIP_{25})$ calibrations

Open Research

The core-top biomarker database investigated for the development of *BaySIC* is available as Supporting Information. The *BaySIC* software package (Python) is publicly available on GitHub via

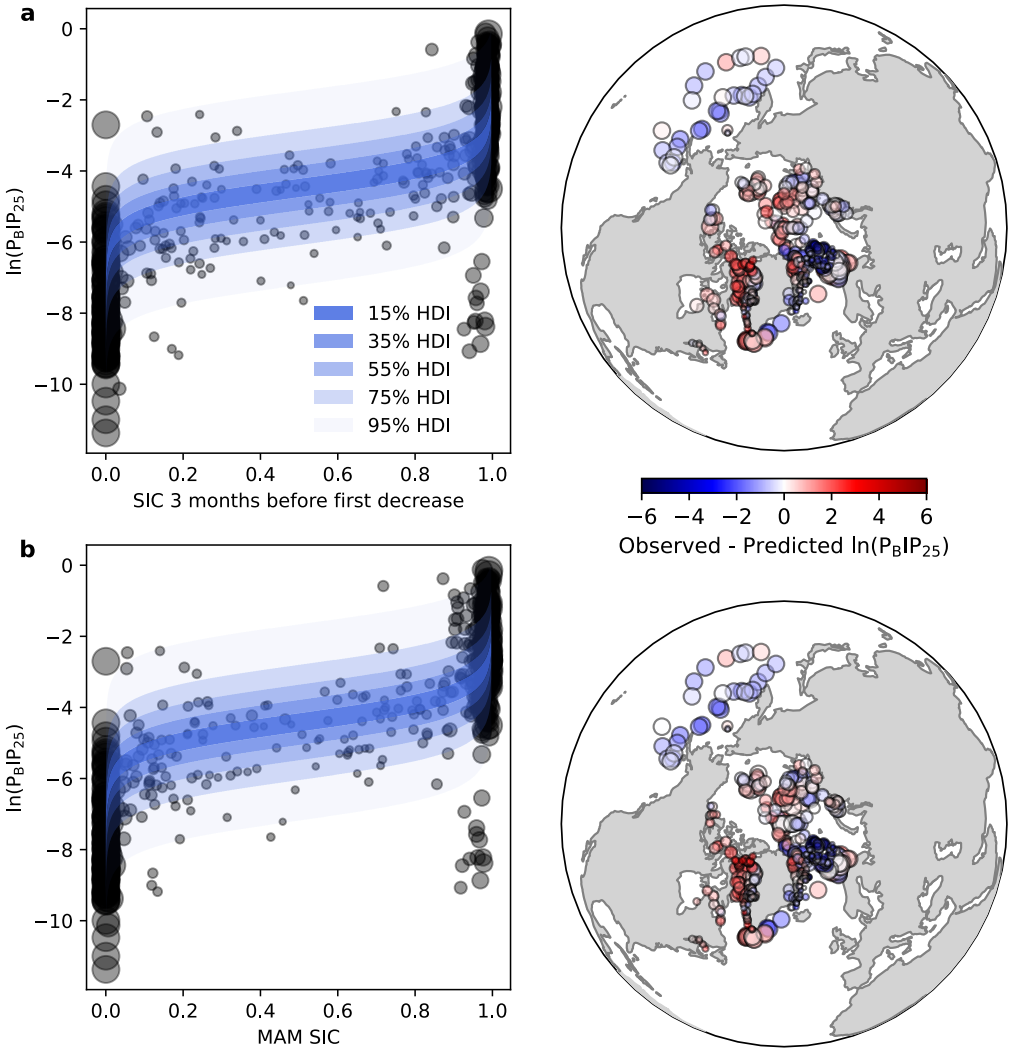

Figure A1. Calibrations (left) for $\ln(P_BIP_{25})$ using the sea ice concentrations (SIC) of (a) the average of the three months before the first SIC decrease and (b) Mar-Apr-May, and the corresponding spatial distributions of residuals (right). Bubble size is inversely proportional to the interquartile range of the SIC over the 22-year calibration period. HDI = highest density interval.

https://github.com/CrystalCYFu/PyBaySIC with the Creative Commons Attribution-NonCommercial 4.0 International License. Both the software and the data are also archived in Zenodo (Fu et al., 2025a, 2025b).

Acknowledgments

We thank Simon Belt for many useful discussions and for help in steering early versions of this manuscript, and Henriette Kolling for graciously sharing IP_{25} and sterol core-top data. We are deeply grateful to the numerous scientists who collected core-top samples from across the Arctic seafloor, measured them in laboratories, and generously made their hard-earned data publicly available. C.Y.F. acknowledges financial support from Girton College (University of Cambridge), Quacquarelli Symonds, and the Cambridge Commonwealth, European & International Trust. Funding for this work was provided by a U.S. NSF Office of Polar Programs grant (OPP-2202667) to M.B.O.

References

Arrigo, K. R., Mock, T., & Lizotte, M. P. (2010). Primary Producers and Sea Ice. In D. N. Thomas & G. S. Dieckmann (Eds.), *Sea Ice* (2nd ed., pp. 283–325). Chichester: Wiley-Blackwell. doi: 10.1002/9781444317145.ch8

Bai, Y., Sicre, M.-A., Chen, J., Klein, V., Jin, H., Ren, J., ... Zhao, M. (2019). Seasonal and spatial variability of sea ice and phytoplankton biomarker flux in the Chukchi sea (western Arctic Ocean). *Progress in Oceanography*, *171*, 22–37. doi: 10.1016/j.pocean.2018.12.002

Belt, S. T. (2018). Source-specific biomarkers as proxies for Arctic and Antarctic sea ice. *Organic Geochemistry*, *125*, 277–298. doi: 10.1016/j.orggeochem.2018.10.002

Belt, S. T., Brown, T. A., Ringrose, A. E., Cabedo-Sanz, P., Mundy, C. J., Gosselin, M., & Poulin, M. (2013). Quantitative measurement of the sea ice diatom biomarker IP25 and sterols in Arctic sea ice and underlying sediments: Further considerations for palaeo sea ice reconstruction. *Organic Geochemistry*, *62*, 33–45. doi: 10.1016/j.orggeochem.2013.07.002

Belt, S. T., Brown, T. A., Smik, L., Assmy, P., & Mundy, C. J. (2018). Sterol identification in floating Arctic sea ice algal aggregates and the Antarctic sea ice diatom *Berkeleya adeliensis*. *Organic Geochemistry*, *118*, 1–3. doi: 10.1016/j.orggeochem.2018.01.008

Belt, S. T., Cabedo-Sanz, P., Smik, L., Navarro-Rodriguez, A., Berben, S. M., Knies, J., & Husum, K. (2015). Identification of paleo Arctic winter sea ice limits and the marginal ice zone: Optimised biomarker-based reconstructions of late Quaternary Arctic sea ice. *Earth and Planetary Science Letters*, *431*, 127–139. doi: 10.1016/j.epsl.2015.09.020

Belt, S. T., Massé, G., Rowland, S. J., Poulin, M., Michel, C., & LeBlanc, B. (2007). A novel chemical fossil of palaeo sea ice: IP25. *Organic Geochemistry*, *38*(1), 16–27. doi: 10.1016/j.orggeochem.2006.09.013

Belt, S. T., Massé, G., Vare, L. L., Rowland, S. J., Poulin, M., Sicre, M.-A., ... Fortier, L. (2008). Distinctive 13C isotopic signature distinguishes a novel sea ice biomarker in Arctic sediments and sediment traps. *Marine Chemistry*, *112*(3-4), 158–167. doi: 10.1016/j.marchem.2008.09.002

Belt, S. T., & Müller, J. (2013). The Arctic sea ice biomarker IP25: a review of current understanding, recommendations for future research and applications in palaeo sea ice reconstructions. *Quaternary Science Reviews*, *79*, 9–25. doi: 10.1016/j.quascirev.2012.12.001

Bliss, A. C., & Anderson, M. R. (2018). Arctic Sea Ice Melt Onset Timing From Passive Microwave-Based and Surface Air Temperature-Based Methods. *Journal of Geophysical Research: Atmospheres*, *123*(17), 9063–9080. doi: 10.1029/2018JD028676

Boyer, T. P., García, H. E., Locarnini, R. A., Zweng, M. M., Mishonov, A. V., Reagan, J. R., ... Smolyar, I. V. (2018). *World Ocean Atlas 2018. Temperature, Salinity, Silicate,*

Phosphate, and Nitrate. NOAA National Centers for Environmental Information. Retrieved from https://www.ncei.noaa.gov/archive/accession/NCEI-WOA18

Brown, T. A., Belt, S. T., Gosselin, M., Levasseur, M., Poulin, M., & Mundy, C. J. (2016). Quantitative estimates of sinking sea ice particulate organic carbon based on the biomarker IP25. *Marine Ecology Progress Series*, *546*, 17–29. doi: 10.3354/meps11668

Brown, T. A., Belt, S. T., Philippe, B., Mundy, C. J., Massé, G., Poulin, M., & Gosselin, M. (2011). Temporal and vertical variations of lipid biomarkers during a bottom ice diatom bloom in the Canadian Beaufort Sea: further evidence for the use of the IP25 biomarker as a proxy for spring Arctic sea ice. *Polar Biol*, *34*(12), 1857–1868. doi: 10.1007/s00300-010-0942-5

Budéus, G. (2007). *Short Cruise Report RV Maria S. Merian Cruise MSM05/5* (Tech. Rep.). University of Hamburg, Institute of Oceanography.

Cabedo-Sanz, P., & Belt, S. T. (2016). Seasonal sea ice variability in eastern Fram Strait over the last 2000 years. *Arktos*, *2*(1), 22. doi: 10.1007/s41063-016-0023-2

Castellani, G., Losch, M., Lange, B. A., & Flores, H. (2017). Modeling Arctic sea-ice algae: Physical drivers of spatial distribution and algae phenology. *Journal of Geophysical Research: Oceans*, *122*(9), 7466–7487. doi: 10.1002/2017JC012828

Christen, J. A., & Fox, C. (2010). A general purpose sampling algorithm for continuous distributions (the t-walk). *Bayesian Analysis*, *5*(2), 263–281. doi: 10.1214/10-BA603

Clotten, C., Fahl, K., Stein, R., & De Schepper, S. (2017). *Organic biomarker records and dinoflagellate cyst concentrations from the Pliocene to earliest Quaternary of ODP Site 907, Iceland Sea* [dataset publication series]. PANGAEA. (Supplement to: Clotten, Caroline; Stein, Ruediger; Fahl, Kirsten; De Schepper, Stijn (2018): Seasonal sea ice cover during the warm Pliocene: Evidence from the Iceland Sea (ODP Site 907). Earth and Planetary Science Letters, 481, 61-72, https://doi.org/10.1016/j.epsl.2017.10.011) doi: 10.1594/PANGAEA.877309

Clotten, C., Stein, R., Fahl, K., & De Schepper, S. (2018). Seasonal sea ice cover during the warm Pliocene: Evidence from the Iceland Sea (ODP Site 907). *Earth and Planetary Science Letters*, *481*, 61–72. doi: 10.1016/j.epsl.2017.10.011

Curry, J. A., Schramm, J. L., & Ebert, E. E. (1995). Sea Ice–Albedo Climate Feedback Mechanism. *Journal of Climate*, *8*(2), 240–247. doi: 10.1175/1520-0442(1995)008⟨0240:SIACFM⟩2.0.CO;2

de Vernal, A., Gersonde, R., Goosse, H., Seidenkrantz, M.-S., & Wolff, E. W. (2013). Sea ice in the paleoclimate system: the challenge of reconstructing sea ice from proxies – an introduction. *Quaternary Science Reviews*, *79*, 1–8. doi: 10.1016/j.quascirev.2013.08.009

de Vernal, A., Hillaire-Marcel, C., Le Duc, C., Roberge, P., Brice, C., Matthiessen, J., ... Stein, R. (2020). Natural variability of the Arctic Ocean sea ice during the present interglacial. *Proceedings of the National Academy of Sciences*, *117*(42), 26069–26075. doi: 10.1073/pnas.2008996117

de Vernal, A., Rochon, A., Fréchette, B., Henry, M., Radi, T., & Solignac, S. (2013). Reconstructing past sea ice cover of the Northern Hemisphere from dinocyst assemblages: status of the approach. *Quaternary Science Reviews*, *79*, 122–134. doi: 10.1016/j.quascirev.2013.06.022

Fahl, K., & Nöthig, E.-M. (2007). Lithogenic and biogenic particle fluxes on the Lomonosov Ridge (central Arctic Ocean) and their relevance for sediment accumulation: Vertical vs. lateral transport. *Deep Sea Research Part I: Oceanographic Research Papers*, *54*(8), 1256–1272. doi: 10.1016/j.dsr.2007.04.014

Fahl, K., & Stein, R. (2012). Modern seasonal variability and deglacial/Holocene change of central Arctic Ocean sea-ice cover: New insights from biomarker proxy records. *Earth and Planetary Science Letters*, *351-352*, 123–133. doi: 10.1016/j.epsl.2012.07.009

Fahl, K., Stein, R., Gaye-Haake, B., Gebhardt, C., Kodina, L. A., Unger, D., & Ittekkot, V. (2003). Biomarkers in surface sediments from the Ob and Yenisei estuaries and the southern Kara Sea: Evidence for particulate organic carbon sources, pathways, and

degradation. In R. Stein, K. Fahl, D. Fütterer, E. Galimov, & O. Stepanets (Eds.), *Siberian river run-off in the kara sea: Characterisation, quantification, variability, and environmental significance* (Vol. 6, pp. 329–348). Amsterdam: Elsevier.

Falardeau, J., de Vernal, A., & Spielhagen, R. F. (2018). Paleoceanography of north-eastern Fram Strait since the last glacial maximum: Palynological evidence of large amplitude changes. *Quaternary Science Reviews*, *195*, 133–152. doi: 10.1016/j.quascirev.2018.06.030

Falardeau, J., de Vernal, A., & Spielhagen, R. F. (2019). Palynological data of cores MSM5/5–712–2 and PS2863/1–2 from northeastern Fram Strait spanning the last glacial maximum to present. *Data in Brief*, *24*, 103899. doi: 10.1016/j.dib.2019.103899

Fu, C. Y., Osman, M., & Aquino-Lopez, M. (2025a). *BaySIC software (Python)* [software]. Zenodo. doi: 10.5281/zenodo.14851610

Fu, C. Y., Osman, M., & Aquino-Lopez, M. (2025b). *Core top biomarker database investigated for the development of BaySIC* [dataset]. Zenodo. doi: 10.5281/zenodo.14824803

Gal, J., Ha, S., Park, J., Shin, K., Kim, D., Kim, N., . . . Yang, E. J. (2022). Seasonal Flux of Ice-Related Organic Matter During Under-Ice Blooms in the Western Arctic Ocean Revealed by Algal Lipid Biomarkers. *JGR Oceans*, *127*(2), e2021JC017914. doi: 10.1029/2021JC017914

Garcia, H. E., Weathers, K., Paver, C. R., Smolyar, I., Boyer, T. P., Locarnini, R. A., . . . Reagan, J. R. (2019). *World Ocean Atlas 2018, Volume 4: Dissolved Inorganic Nutrients (phosphate, nitrate and nitrate+nitrite, silicate).* (Tech. Rep. No. NOAA Atlas NESDIS 84). NOAA National Centers for Environmental Information.

Glud, R. N., Rysgaard, S., Kühl, M., & Hansen, J. W. (2007). The sea ice in Young Sound: Implications for carbon cycling. *Meddr Grønland. Biosci*, *58*, 62–85. doi: 10.7146/mogbiosci.v58.142641

Goad, L. J., Holz, G. G., & Beach, D. H. (1983). Identification of (24*S*)-24-methylcholesta-5,22-dien-3β-ol as the major sterol of a marine cryptophyte and a marine prymnesiophyte. *Phytochemistry*, *22*(2), 475–476. doi: 10.1016/0031-9422(83)83028-3

Gosselin, M., Legendre, L., Therriault, J.-C., Demers, S., & Rochet, M. (1986). Physical control of the horizontal patchiness of sea-ice microalgae. *Mar. Ecol. Prog. Ser.*, *29*, 289–298. doi: 10.3354/meps029289

Gradinger, R. (2009). Sea-ice algae: Major contributors to primary production and algal biomass in the Chukchi and Beaufort Seas during May/June 2002. *Deep Sea Research Part II: Topical Studies in Oceanography*, *56*(17), 1201–1212. doi: 10.1016/j.dsr2.2008.10.016

Grant, W. S., & Horner, R. A. (1976). Growth Responses to Salinity Variation in Four Arctic Ice Diatoms. *Journal of Phycology*, *12*(2), 180–185. doi: 10.1111/j.1529-8817.1976.tb00498.x

Harning, D. J., Holman, B., Woelders, L., Jennings, A. E., & Sepúlveda, J. (2023). Biomarker characterization of the North Water Polynya, Baffin Bay: implications for local sea ice and temperature proxies. *Biogeosciences*, *20*(1), 229–249. doi: 10.5194/bg-20-229-2023

Hoem, F. S., Sauermilch, I., Aleksinski, A. K., Huber, M., Peterse, F., Sangiorgi, F., & Bijl, P. K. (2022). Strength and variability of the Oligocene Southern Ocean surface temperature gradient. *Commun Earth Environ*, *3*(1), 1–8. doi: 10.1038/s43247-022-00666-5

Hoff, U., Rasmussen, T. L., Stein, R., Ezat, M. M., & Fahl, K. (2016). Sea ice and millennial-scale climate variability in the Nordic seas 90 kyr ago to present. *Nat Commun*, *7*(1), 12247. doi: 10.1038/ncomms12247

Horvath, S., Stroeve, J., Rajagopalan, B., & Jahn, A. (2021). Arctic sea ice melt onset favored by an atmospheric pressure pattern reminiscent of the North American-Eurasian Arctic pattern. *Clim Dyn*, *57*(7), 1771–1787. doi: 10.1007/s00382-021-05776-y

Hörner, T., Stein, R., Fahl, K., & Birgel, D. (2016). Post-glacial variability of sea ice cover,

river run-off and biological production in the western Laptev Sea (Arctic Ocean) – A high-resolution biomarker study. *Quaternary Science Reviews*, *143*, 133–149. doi: 10.1016/j.quascirev.2016.04.011

Ivanov, V., Varentsov, M., Matveeva, T., Repina, I., Artamonov, A., & Khavina, E. (2019). Arctic Sea Ice Decline in the 2010s: The Increasing Role of the Ocean—Air Heat Exchange in the Late Summer. *Atmosphere*, *10*(4), 184. doi: 10.3390/atmos10040184

Ji, R., Jin, M., & Varpe, Ø. (2013). Sea ice phenology and timing of primary production pulses in the Arctic Ocean. *Global Change Biology*, *19*(3), 734–741. doi: 10.1111/gcb.12074

Karami, M. P., Myers, P. G., de Vernal, A., Tremblay, L. B., & Hu, X. (2021). The role of Arctic gateways on sea ice and circulation in the Arctic and North Atlantic Oceans: a sensitivity study with an ocean-sea-ice model. *Clim Dyn*, *57*(7), 2129–2151. doi: 10.1007/s00382-021-05798-6

Knies, J., Cabedo-Sanz, P., Belt, S. T., Baranwal, S., Fietz, S., & Rosell-Melé, A. (2014). The emergence of modern sea ice cover in the Arctic Ocean. *Nat Commun*, *5*(1), 5608. doi: 10.1038/ncomms6608

Koch, C. W., Cooper, L. W., Lalande, C., Brown, T. A., Frey, K. E., & Grebmeier, J. M. (2020). Seasonal and latitudinal variations in sea ice algae deposition in the Northern Bering and Chukchi Seas determined by algal biomarkers. *PLOS ONE*, *15*(4), e0231178. doi: 10.1371/journal.pone.0231178

Kolling, H. M., Stein, R., Fahl, K., Sadatzki, H., de Vernal, A., & Xiao, X. (2020). Biomarker Distributions in (Sub)-Arctic Surface Sediments and Their Potential for Sea Ice Reconstructions. *Geochem Geophys Geosyst*, *21*(10), e2019GC008629. doi: 10.1029/2019GC008629

Kremer, A., Stein, R., & Fahl, K. (2018). *Organic-geochemical bulk parameter and biomarker distribution of sediment core PS92/039-2* [dataset publication series]. PANGAEA. (Supplement to: Kremer, Anne; Stein, Ruediger; Fahl, Kirsten; Ji, Z; Yang, Z; Wiers, Steffen; Matthiessen, Jens; Forwick, Matthias; Löwemark, Ludvig; O'Regan, Matthew; Chen, Jiaming; Snowball, Ian (2018): Changes in sea ice cover and ice sheet extent at the Yermak Plateau during the last 160 ka - Reconstructions from biomarker records. Quaternary Science Reviews, 182, 93-108, https://doi.org/10.1016/j.quascirev.2017.12.016) doi: 10.1594/PANGAEA.884795

Kremer, A., Stein, R., Fahl, K., Bauch, H., Mackensen, A., & Niessen, F. (2018). A 190-ka biomarker record revealing interactions between sea ice, Atlantic Water inflow and ice sheet activity in eastern Fram Strait. *Arktos*, *4*(1), 1–17. doi: 10.1007/s41063-018-0052-0

Kremer, A., Stein, R., Fahl, K., Ji, Z., Yang, Z., Wiers, S., ... Snowball, I. (2018). Changes in sea ice cover and ice sheet extent at the Yermak Plateau during the last 160 ka – Reconstructions from biomarker records. *Quaternary Science Reviews*, *182*, 93–108. doi: 10.1016/j.quascirev.2017.12.016

Kullback, S., & Leibler, R. A. (1951). On Information and Sufficiency. *The Annals of Mathematical Statistics*, *22*(1), 79–86. doi: 10.1214/aoms/1177729694

Köseoğlu, D. (2019). *Development of biomarker-based proxy methods for reconstructing the late Quaternary sea ice history in the Barents Sea* (Doctoral dissertation, School of Geography, Earth and Environmental Sciences, University of Plymouth). doi: 10.24382/1109

Lalande, C., Nöthig, E.-M., Bauerfeind, E., Hardge, K., Beszczynska-Möller, A., & Fahl, K. (2016). Lateral supply and downward export of particulate matter from upper waters to the seafloor in the deep eastern Fram Strait. *Deep Sea Research Part I: Oceanographic Research Papers*, *114*, 78–89. doi: 10.1016/j.dsr.2016.04.014

Lavoie, D., Denman, K., & Michel, C. (2005). Modeling ice algal growth and decline in a seasonally ice-covered region of the Arctic (Resolute Passage, Canadian Archipelago). *Journal of Geophysical Research: Oceans*, *110*(C11). doi: 10.1029/2005JC002922

Legendre, L., Ackley, S. F., Dieckmann, G. S., Gulliksen, B., Horner, R., Hoshiai, T., ... Sullivan, C. W. (1992). Ecology of sea ice biota. *Polar Biol*, *12*(3), 429–444. doi:

10.1007/BF00243114

Leu, E., Mundy, C. J., Assmy, P., Campbell, K., Gabrielsen, T. M., Gosselin, M., ... Gradinger, R. (2015). Arctic spring awakening – Steering principles behind the phenology of vernal ice algal blooms. *Progress in Oceanography*, *139*, 151–170. doi: 10.1016/j.pocean.2015.07.012

Leu, E., Søreide, J. E., Hessen, D. O., Falk-Petersen, S., & Berge, J. (2011). Consequences of changing sea-ice cover for primary and secondary producers in the European Arctic shelf seas: Timing, quantity, and quality. *Progress in Oceanography*, *90*(1), 18–32. doi: 10.1016/j.pocean.2011.02.004

Limoges, A., Massé, G., Weckström, K., Poulin, M., Ellegaard, M., Heikkilä, M., ... Ribeiro, S. (2018). Spring Succession and Vertical Export of Diatoms and IP25 in a Seasonally Ice-Covered High Arctic Fjord. *Front. Earth Sci.*, *6*, 226. doi: 10.3389/feart.2018.00226

Liu, Z., Otto-Bliesner, B. L., He, F., Brady, E. C., Tomas, R., Clark, P. U., ... Cheng, J. (2009). Transient Simulation of Last Deglaciation with a New Mechanism for Bølling-Allerød Warming. *Science*, *325*(5938), 310–314. doi: 10.1126/science.1171041

Locarnini, R. A., Mishonov, A. V., Baranova, O. K., Boyer, T. P., Zweng, M. M., Garcia, H. E., ... Smolyar, I. (2019). *World Ocean Atlas 2018, Volume 1: Temperature.* (Tech. Rep. No. NOAA Atlas NESDIS 81). NOAA National Centers for Environmental Information.

Luostarinen, T., Weckström, K., Ehn, J., Kamula, M., Burson, A., Diaz, A., ... Heikkilä, M. (2023). Seasonal and habitat-based variations in vertical export of biogenic sea-ice proxies in Hudson Bay. *Commun Earth Environ*, *4*(1), 1–13. doi: 10.1038/s43247-023-00719-3

Malevich, S. B., Vetter, L., & Tierney, J. E. (2019). Global Core Top Calibration of δ^{18}O in Planktic Foraminifera to Sea Surface Temperature. *Paleoceanog and Paleoclimatol*, *34*(8), 1292–1315. doi: 10.1029/2019PA003576

Markus, T., Stroeve, J. C., & Miller, J. (2009). Recent changes in Arctic sea ice melt onset, freezeup, and melt season length. *Journal of Geophysical Research: Oceans*, *114*(C12). doi: 10.1029/2009JC005436

Mauritzen, C., & Häkkinen, S. (1997). Influence of sea ice on the thermohaline circulation in the Arctic-North Atlantic Ocean. *Geophysical Research Letters*, *24*(24), 3257–3260. doi: 10.1029/97GL03192

Meier, W. N., Fetterer, F., Windnagel, A. K., & Stewart, J. S. (2021). *NOAA/NSIDC Climate Data Record of Passive Microwave Sea Ice Concentration, Version 4.* NSIDC. doi: 10.7265/EFMZ-2T65

Mortin, J., Svensson, G., Graversen, R. G., Kapsch, M.-L., Stroeve, J. C., & Boisvert, L. N. (2016). Melt onset over Arctic sea ice controlled by atmospheric moisture transport. *Geophysical Research Letters*, *43*(12), 6636–6642. doi: 10.1002/2016GL069330

Mundy, C. J., Barber, D. G., & Michel, C. (2005). Variability of snow and ice thermal, physical and optical properties pertinent to sea ice algae biomass during spring. *Journal of Marine Systems*, *58*(3), 107–120. doi: 10.1016/j.jmarsys.2005.07.003

Méheust, M., Fahl, K., & Stein, R. (2013). Variability in modern sea surface temperature, sea ice and terrigenous input in the sub-polar North Pacific and Bering Sea: Reconstruction from biomarker data. *Organic Geochemistry*, *57*, 54–64. doi: 10.1016/j.orggeochem.2013.01.008

Müller, J., Massé, G., Stein, R., & Belt, S. T. (2009). Variability of sea-ice conditions in the Fram Strait over the past 30,000 years. *Nature Geosci*, *2*(11), 772–776. doi: 10.1038/ngeo665

Müller, J., & Stein, R. (2014). High-resolution record of late glacial and deglacial sea ice changes in Fram Strait corroborates ice–ocean interactions during abrupt climate shifts. *Earth and Planetary Science Letters*, *403*, 446–455. doi: 10.1016/j.epsl.2014.07.016

Müller, J., & Stein, R. (2014). *Late glacial and deglacial age model and biomarker analyses of sediment core MSM05/5_712-2 from the western continental slope of*

Svalbard [dataset]. PANGAEA. (Supplement to: Müller, J; Stein, R (2014): High-resolution record of late glacial and deglacial sea ice changes in Fram Strait corroborates ice-ocean interactions during abrupt climate shifts. Earth and Planetary Science Letters, 403, 446-455, https://doi.org/10.1016/j.epsl.2014.07.016) doi: 10.1594/PANGAEA.833668

Müller, J., Wagner, A., Fahl, K., Stein, R., Prange, M., & Lohmann, G. (2011). Towards quantitative sea ice reconstructions in the northern North Atlantic: A combined biomarker and numerical modelling approach. *Earth and Planetary Science Letters*, *306*(3), 137–148. doi: 10.1016/j.epsl.2011.04.011

Müller, J., Werner, K., Stein, R., Fahl, K., Moros, M., & Jansen, E. (2012). *Age determinations, biomarker analyses, and accumulation rates of three sediment cores from the Fram Strait* [dataset publication series]. PANGAEA. (Supplement to: Müller, J et al. (2012): Holocene cooling culminates in sea ice oscillations in Fram Strait. Quaternary Science Reviews, 47, 1-14, https://doi.org/10.1016/j.quascirev.2012.04.024) doi: 10.1594/PANGAEA.779628

Müller, J., Werner, K., Stein, R., Fahl, K., Moros, M., & Jansen, E. (2012). Holocene cooling culminates in sea ice oscillations in Fram Strait. *Quaternary Science Reviews*, *47*, 1–14. doi: 10.1016/j.quascirev.2012.04.024

Navarro-Rodriguez, A., Belt, S. T., Knies, J., & Brown, T. A. (2013). Mapping recent sea ice conditions in the Barents Sea using the proxy biomarker IP25: implications for palaeo sea ice reconstructions. *Quaternary Science Reviews*, *79*, 26–39. doi: 10.1016/j.quascirev.2012.11.025

Nichols, P. D., Jones, G. J., De Leeuw, J. W., & Johns, R. B. (1984). The fatty acid and sterol composition of two marine dinoflagellates. *Phytochemistry*, *23*(5), 1043–1047. doi: 10.1016/S0031-9422(00)82605-9

Notz, D., & SIMIP Community. (2020). Arctic Sea Ice in CMIP6. *Geophysical Research Letters*, *47*(10), e2019GL086749. doi: 10.1029/2019GL086749

Nöthig, E.-M., Lalande, C., Fahl, K., Metfies, K., Salter, I., & Bauerfeind, E. (2020). Annual cycle of downward particle fluxes on each side of the Gakkel Ridge in the central Arctic Ocean. *Phil. Trans. R. Soc. A.*, *378*(2181), 20190368. doi: 10.1098/rsta.2019.0368

Osman, M. B., Tierney, J. E., Zhu, J., Tardif, R., Hakim, G. J., King, J., & Poulsen, C. J. (2021). Globally resolved surface temperatures since the Last Glacial Maximum. *Nature*, *599*(7884), 239–244. doi: 10.1038/s41586-021-03984-4

Oziel, L., Massicotte, P., Randelhoff, A., Ferland, J., Vladoiu, A., Lacour, L., ... Babin, M. (2019). Environmental factors influencing the seasonal dynamics of spring algal blooms in and beneath sea ice in western Baffin Bay. *Elementa: Science of the Anthropocene*, *7*, 34. doi: 10.1525/elementa.372

Pieńkowski, A. J., Gill, N. K., Furze, M. F., Mugo, S. M., Marret, F., & Perreaux, A. (2017). Arctic sea-ice proxies: Comparisons between biogeochemical and micropalaeontological reconstructions in a sediment archive from Arctic Canada. *The Holocene*, *27*(5), 665–682. doi: 10.1177/0959683616670466

Ralph, P. J., Ryan, K. G., Martin, A., & Fenton, G. (2007). Melting out of sea ice causes greater photosynthetic stress in algae than freezing in. *Journal of Phycology*, *43*(5), 948–956. doi: 10.1111/j.1529-8817.2007.00382.x

Ribeiro, S., Sejr, M. K., Limoges, A., Heikkilä, M., Andersen, T. J., Tallberg, P., ... Rysgaard, S. (2017). Sea ice and primary production proxies in surface sediments from a High Arctic Greenland fjord: Spatial distribution and implications for palaeoenvironmental studies. *Ambio*, *46*(S1), 106–118. doi: 10.1007/s13280-016-0894-2

Rontani, J.-F., Belt, S. T., Brown, T. A., Amiraux, R., Gosselin, M., Vaultier, F., & Mundy, C. J. (2016). Monitoring abiotic degradation in sinking versus suspended Arctic sea ice algae during a spring ice melt using specific lipid oxidation tracers. *Organic Geochemistry*, *98*, 82–97. doi: 10.1016/j.orggeochem.2016.05.016

Rysgaard, S., Bendtsen, J., Delille, B., Dieckmann, G. S., Glud, R. N., Kennedy, H., ... Tison, J.-L. (2011). Sea ice contribution to the air–sea CO2 exchange in the Arctic and Southern Oceans. *Tellus B*, *63*(5), 823–830. doi: 10.1111/j.1600-0889.2011.00571.x

Rózańska, M., Gosselin, M., Poulin, M., Wiktor, J., & Michel, C. (2009). Influence of environmental factors on the development of bottom ice protist communities during the winter–spring transition. *Mar. Ecol. Prog. Ser.*, *386*, 43–59. doi: 10.3354/meps08092

Salter, I., Bauerfeind, E., Fahl, K., Iversen, M. H., Lalande, C., Ramondenc, S., ... Nöthig, E.-M. (2023). Interannual variability (2000–2013) of mesopelagic and bathypelagic particle fluxes in relation to variable sea ice cover in the eastern Fram Strait. *Front. Earth Sci.*, *11*, 1210213. doi: 10.3389/feart.2023.1210213

Sime, L. C., Sivankutty, R., Vallet-Malmierca, I., de Boer, A. M., & Sicard, M. (2023). Summer surface air temperature proxies point to near-sea-ice-free conditions in the Arctic at 127 ka. *Climate of the Past*, *19*(4), 883–900. doi: 10.5194/cp-19-883-2023

Smik, L., Cabedo-Sanz, P., & Belt, S. T. (2016). Semi-quantitative estimates of paleo Arctic sea ice concentration based on source-specific highly branched isoprenoid alkenes: A further development of the PIP25 index. *Organic Geochemistry*, *92*, 63–69. doi: 10.1016/j.orggeochem.2015.12.007

Stein, R. (2008). Chapter Six Quaternary Variability of Palaeoenvironment and Its Sedimentary Record. In R. Stein (Ed.), *Arctic Ocean Sediments: Processes, Proxies, and Paleoenvironment* (Vol. 2, pp. 287–437). Amsterdam: Elsevier. doi: 10.1016/S1572-5480(08)00006-7

Stein, R., & Fahl, K. (2013). Biomarker proxy shows potential for studying the entire Quaternary Arctic sea ice history. *Organic Geochemistry*, *55*, 98–102. doi: 10.1016/j.orggeochem.2012.11.005

Stein, R., Fahl, K., Gierz, P., Niessen, F., & Lohmann, G. (2017). Arctic Ocean sea ice cover during the penultimate glacial and the last interglacial. *Nat Commun*, *8*(1), 373. doi: 10.1038/s41467-017-00552-1

Stein, R., Fahl, K., Gierz, P., Niessen, F., & Lohmann, G. (2017). *Biomarker data of four sediment cores from the Arctic Ocean* [dataset publication series]. PANGAEA. (Supplement to: Stein, R et al. (2017): Arctic Ocean sea ice cover during the penultimate glacial and the last interglacial. Nature Communications, 8(1), 13 pp, https://doi.org/10.1038/s41467-017-00552-1) doi: 10.1594/PANGAEA.874357

Stein, R., Fahl, K., Schade, I., Manerung, A., Wassmuth, S., Niessen, F., & Nam, S.-I. (2017). Holocene variability in sea ice cover, primary production, and Pacific-Water inflow and climate change in the Chukchi and East Siberian Seas (Arctic Ocean). *Journal of Quaternary Science*, *32*(3), 362–379. doi: 10.1002/jqs.2929

Stein, R., Fahl, K., Schreck, M., Knorr, G., Niessen, F., Forwick, M., ... Lohmann, G. (2016). Evidence for ice-free summers in the late Miocene central Arctic Ocean. *Nat Commun*, *7*(1), 11148. doi: 10.1038/ncomms11148

Stein, R., Kremer, A., & Fahl, K. (2018). *Biomarker distribution of sediment core PS93/006-1* [dataset publication series]. PANGAEA. (Supplement to: Kremer, Anne; Stein, Ruediger; Fahl, Kirsten; Bauch, Henning A; Mackensen, Andreas; Niessen, Frank (2018): A 190-ka biomarker record revealing interactions between sea ice, Atlantic Water inflow and ice sheet activity in eastern Fram Strait. arktos - The Journal of Arctic Geosciences, 4(1), https://doi.org/10.1007/s41063-018-0052-0) doi: 10.1594/PANGAEA.884799

Steinsland, K., Grant, D., Ninnemann, U. S., Fahl, K., Stein, R., & De Schepper, S. (2023). *Last Interglacial biomarker, dinoflagellate cyst, and stable oxygen isotope data from sediment core GS16-204-22CC-B* [dataset bundled publication]. PANGAEA. doi: 10.1594/PANGAEA.955398

Steinsland, K., Grant, D. M., Ninnemann, U. S., Fahl, K., Stein, R., & De Schepper, S. (2023). Sea ice variability in the North Atlantic subpolar gyre throughout the Last Interglacial. *Quaternary Science Reviews*, *313*, 108198. doi: 10.1016/j.quascirev.2023.108198

Stoynova, V., Shanahan, T. M., Hughen, K. A., & de Vernal, A. (2013). Insights into Circum-Arctic sea ice variability from molecular geochemistry. *Quaternary Science Reviews*, *79*, 63–73. doi: 10.1016/j.quascirev.2012.10.006

Stroeve, J., & Notz, D. (2018). Changing state of Arctic sea ice across all seasons. *Environ.*

Res. Lett., *13*(10), 103001. doi: 10.1088/1748-9326/aade56

Su, L., Ren, J., Sicre, M., Bai, Y., Jalali, B., Li, Z., ... Chen, J. (2022). HBIs and Sterols in Surface Sediments Across the East Siberian Sea: Implications for Palaeo Sea-Ice Reconstructions. *Geochem Geophys Geosyst*, *23*(2), e2021GC009940. doi: 10.1029/2021GC009940

Søgaard, D. H., Hansen, P. J., Rysgaard, S., & Glud, R. N. (2011). Growth limitation of three Arctic sea ice algal species: effects of salinity, pH, and inorganic carbon availability. *Polar Biol*, *34*(8), 1157–1165. doi: 10.1007/s00300-011-0976-3

Tierney, J. E., Malevich, S. B., Gray, W., Vetter, L., & Thirumalai, K. (2019). Bayesian Calibration of the Mg/Ca Paleothermometer in Planktic Foraminifera. *Paleoceanog and Paleoclimatol*, *34*(12), 2005–2030. doi: 10.1029/2019PA003744

Tierney, J. E., & Tingley, M. P. (2014). A Bayesian, spatially-varying calibration model for the TEX86 proxy. *Geochimica et Cosmochimica Acta*, *127*, 83–106. doi: 10.1016/j.gca.2013.11.026

Tierney, J. E., & Tingley, M. P. (2018). BAYSPLINE: A New Calibration for the Alkenone Paleothermometer. *Paleoceanog and Paleoclimatol*, *33*(3), 281–301. doi: 10.1002/2017PA003201

Timm, O., Timmermann, A., Abe-Ouchi, A., Saito, F., & Segawa, T. (2008). On the definition of seasons in paleoclimate simulations with orbital forcing. *Paleoceanography*, *23*(2). doi: 10.1029/2007PA001461

Truong, C., Oudre, L., & Vayatis, N. (2020). Selective review of offline change point detection methods. *Signal Processing*, *167*, 107299. doi: 10.1016/j.sigpro.2019.107299

Vermassen, F., O'Regan, M., de Boer, A., Schenk, F., Razmjooei, M., West, G., ... Coxall, H. K. (2023). A seasonally ice-free Arctic Ocean during the Last Interglacial. *Nat. Geosci.*, *16*(8), 723–729. doi: 10.1038/s41561-023-01227-x

Volkman, J. K. (1986). A review of sterol markers for marine and terrigenous organic matter. *Organic Geochemistry*, *9*(2), 83–99. doi: 10.1016/0146-6380(86)90089-6

Volkman, J. K., Barrett, S. M., Blackburn, S. I., Mansour, M. P., Sikes, E. L., & Gelin, F. (1998). Microalgal biomarkers: A review of recent research developments. *Organic Geochemistry*, *29*(5-7), 1163–1179. doi: 10.1016/S0146-6380(98)00062-X

Volkman, J. K., Barrett, S. M., Dunstan, G. A., & Jeffrey, S. W. (1993). Geochemical significance of the occurrence of dinosterol and other 4-methyl sterols in a marine diatom. *Organic Geochemistry*, *20*(1), 7–15. doi: 10.1016/0146-6380(93)90076-N

Walsh, J., Chapman, W., & Fetterer, F. (2019). *Gridded Monthly Sea Ice Extent and Concentration, 1850 Onward, Version 2.* NSIDC. doi: 10.7265/JJ4S-TQ79

Wegner, C., Bennett, K. E., de Vernal, A., Forwick, M., Fritz, M., Heikkilä, M., ... Werner, K. (2015). Variability in transport of terrigenous material on the shelves and the deep Arctic Ocean during the Holocene. *Polar Research*. doi: 10.3402/polar.v34.24964

Xiao, X., Fahl, K., Müller, J., & Stein, R. (2015). Sea-ice distribution in the modern Arctic Ocean: Biomarker records from trans-Arctic Ocean surface sediments. *Geochimica et Cosmochimica Acta*, *155*, 16–29. doi: 10.1016/j.gca.2015.01.029

Xiao, X., Fahl, K., & Stein, R. (2013). Biomarker distributions in surface sediments from the Kara and Laptev seas (Arctic Ocean): indicators for organic-carbon sources and sea-ice coverage. *Quaternary Science Reviews*, *79*, 40–52. doi: 10.1016/j.quascirev.2012.11.028

Zhang, Q., Gradinger, R., & Spindler, M. (1999). Experimental study on the effect of salinity on growth rates of Arctic-sea-ice algae from the Greenland Sea. *Boreal environ. res*, *4*(1), 1–8.

Zweng, M. M., Reagan, J. R., Seidov, D., Boyer, T. P., Locarnini, R. A., Garcia, H. E., ... Smolyar, I. (2019). *World Ocean Atlas 2018, Volume 2: Salinity.* (Tech. Rep. No. NOAA Atlas NESDIS 82). NOAA National Centers for Environmental Information.